AD-A090 054 WASHINGTON UNIV SEATTLE APPLIED PHYSICS LAB F/G 8/10
ACOUSTICS AND PROPERTIES OF THE OCEAN: A PRESENTATION TO THE PL--ETC(U)
SEP 80 M SCHULKIN N00014-77-C-0309
UNCLASSIFIED APL-UW-TN-9-80 NL

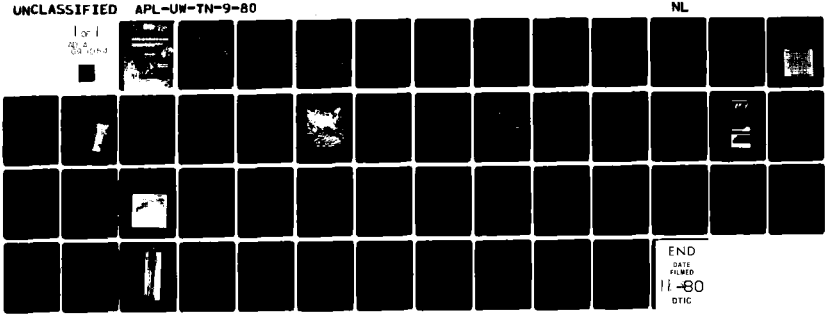

END
DATE FILMED
11-80
DTIC

Contract N00014-77-C-0309

APPLIED • PHYSICS • LABORATORY

A DIVISION OF THE UNIVERSITY OF WASHINGTON

(12)

(6)

ACOUSTICS AND PROPERTIES OF THE OCEAN:

A Presentation to the Plenary Session of OCEANS '80, held at Seattle, Washington, 8 September 1980.

Contract (15) N00014-77-C-0309

(10) by M. Schulkin

(14) APL-UW-TN-9-80

(11) September 1980

(12) 51

ACKNOWLEDGMENTS

The author expresses his appreciation to Mr. R.S. Winokur of the Office of Naval Research and Dr. S.R. Murphy, Director of the Applied Physics Laboratory of the University of Washington, for illuminating reviews of the material presented here. He also owes much to the participants in the NOAA Ocean Acoustic Remote Sensing Workshop held in Seattle in January 1980. In addition, specific help was furnished by Messrs. W. Woodward and J.W. Sherman III of NOAA, and Mr. W.C. Acker, Dr. D.R. Jackson and Dr. T.B. Sanford of APL-UW. Financial and technical support was furnished by Dr. A.O. Sykes of ONR and Dr. H.J. McClellan of the NOAA Sea Grant Office.

ABSTRACT

Acoustical techniques are being used to determine properties of the ocean for scientific and engineering applications. This paper reports on existing concepts and problems in the application of acoustics to oceanic chemistry, geology, biology and dynamics which can be treated in the next decade. By using different regions of the acoustic spectrum and different acoustic path configurations, information can be obtained concerning such topics as climate and weather, fisheries, ocean pollution, bathymetry and currents. These subjects were discussed in the recent NOAA Workshop on Ocean Acoustic Remote Sensing (Seattle, January 1980).

CONTENTS

FIGURE CAPTIONS

I. INTRODUCTION

An ocean acoustical science and technology base now exists which, with proper attention and support, can furnish us with sophisticated tools for monitoring and exploiting the great ocean resources necessary for man's development in the next decade and beyond. It is fortunate that NASA, NOAA, and the Navy are united and coordinated in this effort (Refs. I-1, 2, 3, 4).

The next decade will be an age marrying electromagnetic and acoustical techniques. The vast and quick reconnaissance of ocean areas by satellite will enable locating important ocean phenomena for follow-up detailed aircraft and ocean acoustic remote sensing measurements using buoys, ships with hull-mounted and towed systems, and bottom-based systems. Emphasis will move from static temperature, salinity and sound speed measurements to dynamic measurements of currents, current shear profiles, waves and mixing events such as ring eddies, finestructure and microstructure. The science of ocean particulates will also receive greater attention. As discussed in the NOAA Workshop on Ocean Acoustic Remote Sensing in Seattle in January (Ref. I-2), we will have tools for applying this information to: Climate and Weather, Fisheries, Pollution and Navigation, as well as Energy, Transportation, Recreation, Construction, Mining, Chemicals and Medicines.

My intention in this lecture is to present an up-to-date, brief and balanced survey of the uses of ocean acoustic remote sensing techniques in the study of the subjects listed in Figure I-1. I plan to present about four topics under each subject.

Figure I-1: Ocean Properties

1. MARINE GEOLOGY AND OCEAN DEPTHS
2. OCEAN CHEMISTRY AND POLLUTION
3. BIOMASS AND FISHERIES
4. OCEAN DYNAMICS -- MACROSCALE, SYNOPTIC SCALE, MESOSCALE
5. OCEAN DYNAMICS -- INTERNAL WAVES AND TIDES
6. OCEAN DYNAMICS -- SEA SURFACE AND NEAR-SURFACE LAYER
7. OCEAN DYNAMICS -- FINESTRUCTURE AND MICROSTRUCTURE

Fig. I-1

Figure I-2: Attenuation of Waves in Seawater

As you have heard in the previous paper, satellite oceanography is a great reconnaissance tool. However, it is complementary to ocean acoustic remote sensing. To measure events inside the ocean, one must use acoustical systems. The reason for this is shown in this figure. The electrical conductivity of seawater makes it a much more absorbing medium for radio waves and microwaves. In the figure, I have plotted attenuation in decibels per meter vs decreasing wavelength in meters for both electromagnetic and acoustic waves. It isn't until we get well into the infrared region that optical techniques become competitive with acoustical techniques. We will return to this figure when we discuss the chemistry of acoustic absorption.

Fig. I-2

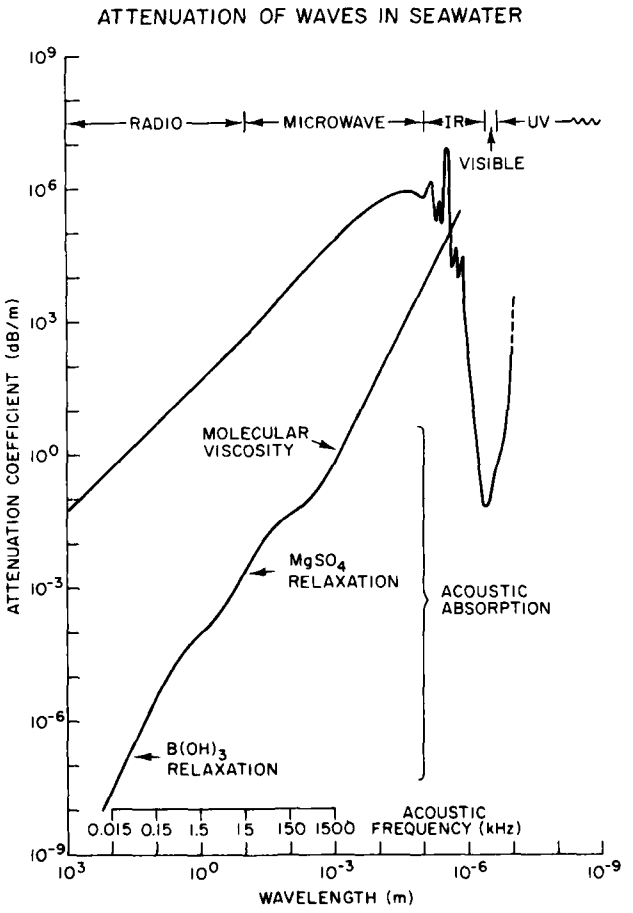

Figure I-3: Satellite Remote Sensing -- Mesoscale Ocean Topography

Some scales of ocean configurations and motions are introduced in the next figure (Ref. I-4), borrowed from the previous speaker, which shows sea surface topography as observed by a satellite. A satellite at 800 km elevation orbits the earth in about 103 minutes, or 14 times a day, overseeing a different earth's track each time. The earth's circumference being 40,000 km, it takes 10 minutes to traverse the 4000 km section of the North Atlantic shown. Note that the apparent sea level is depressed by about 15 m due to the Puerto Rico Trench. The smallest horizontal dynamic features resolved here are mesoscale features of the order of 10 km or more, e.g. the Gulf Stream width and a warm eddy. The Gulf Stream shows a dynamic height of a couple of meters, while that of the warm core eddy is about a meter.

SATELLITE REMOTE SENSING -- MESOSCALE OCEAN TOPOGRAPHY

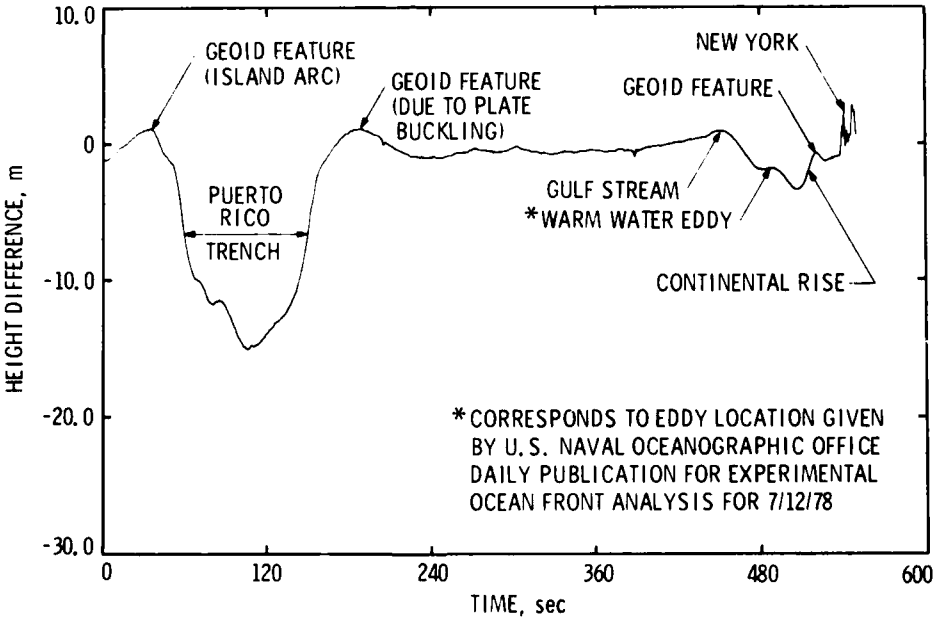

[DIFFERENCE OF SEASAT ALTIMETER SEA SURFACE HEIGHT AND GEM 10B GEOID FOR NORTH ATLANTIC PASS (7/10/78, REV 191)]

Fig. I-3

II. MARINE GEOLOGY AND OCEAN DEPTHS

Identifiable geoidal features such as seamounts and trenches show up well in the figure. Suspected uncharted geoidal features can be investigated by ocean acoustic remote sensing methods, such as echo-sounding or underwater reconnaissance.

Figure II-1: Underwater Topographic Reconnaissance

A method of underwater reconnaissance for seamounts has been developed at the Naval Research Laboratory (Ref. II-1). This method uses 50 lb charges at depths of 1000-1500 m and a ship-towed receiving array at 300 m depth to explore areas as large as a million square nautical miles. The figure shows a processed map of reverberation returns, in the 100-130 Hz band, from seamounts and ridges in the New Zealand area. The map was produced by overlaying 20 single shot results and can be prepared on-line. The scale of the longitude-latitude grid is 1° x 1°. The highlights on the right side are a chain of uncharted seamounts, composing the Louisville Ridge. This new fact was verified by the New Zealand Navy. Such acoustic remote sensing reconnaissance can be done in conjunction with satellite surveys.

Figure II-2: Echosounding, Shallow Penetration Subbottom Profiling, and Seismic Profiling

Ship echosounders are used to verify the details of seamounts. Echosounders measure depth by timing the interval between the emission of a pulse and the echo return. This figure illustrates three adaptations of this device for: (1) echosounding (12 kHz); (2) shallow penetration subbottom profiling (3.5 kHz to 200 m); and (3) seismic profiling (broadband low frequency sources). In the last case, the record was received at 25 Hz. One second of time corresponds to a depth of 1 or more kilometers in the bottom (two way travel). One tenth of a second corresponds to about 100 m. The return averages the depth over a footprint at the bottom. The footprint here is 260 m for a 5° beam in 3000 m of water.

Figure II-3: Types of Sonar for Sensing Sea Floor and Subbottom (Ref. II-3)

Fig. II-3

- ECHOSOUNDER
- SHALLOW-PENETRATION SUBBOTTOM PROFILER
- SEISMIC PROFILER
- SWATH-MAPPING SONAR
- SIDE-LOOKING SONAR

Swath-mapping sonar is an echosounding system with areal coverage and higher speed capabilities. One type, called SEABEAM, is a stabilized multi-narrow-beam system that provides fan coverage athwartships. Side-looking sonar provides the ability to portray bottom roughness distributions, small irregularities and bottom obstructions. It is usually a very high frequency system (125 kHz) and towed near the bottom.

Most of the listed system types have high-frequency deeply-towed versions to get higher resolution. Shallow water systems are usually hull-mounted. Future developments in marine geoacoustics could include subbottom holography, and the monitoring of seafloor spreading with an array of acoustic transponders and precision timing devices (Ref. II-3).

UNDERWATER TOPOGRAPHIC RECONNAISSANCE (NRL):
DISCOVERY OF SEAMOUNT CHARACTER OF LOUISVILLE RIDGE, NEW ZEALAND

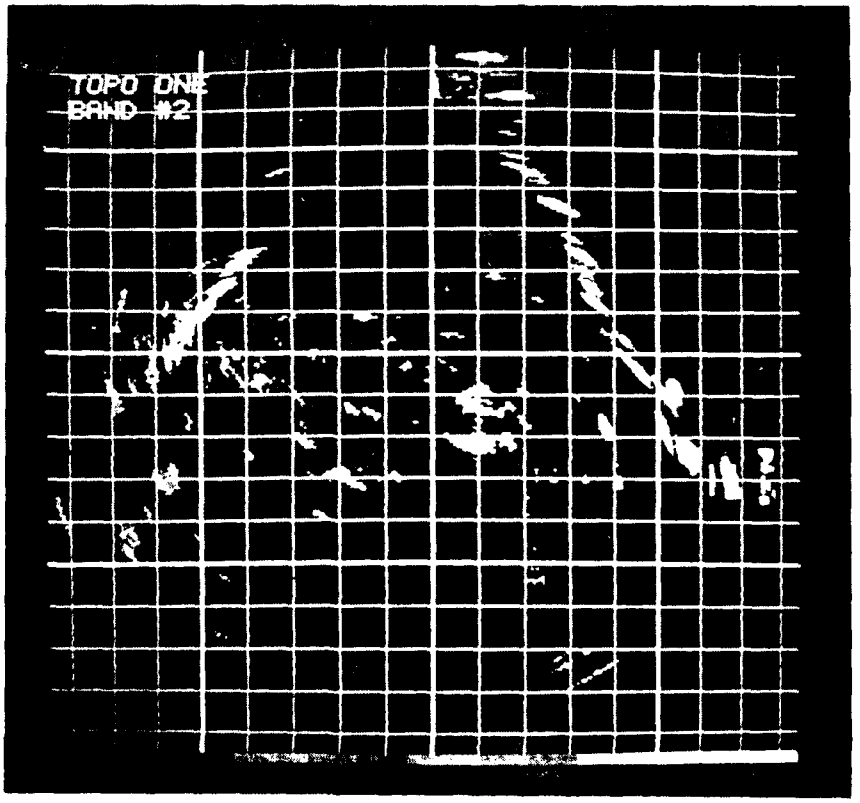

Fig. II-1

(Schifter et al.: 1979)

Fig. II-2

ECHOSOUNDING, SHALLOW PENETRATION SUBBOTTOM PROFILING AND SEISMIC PROFILING

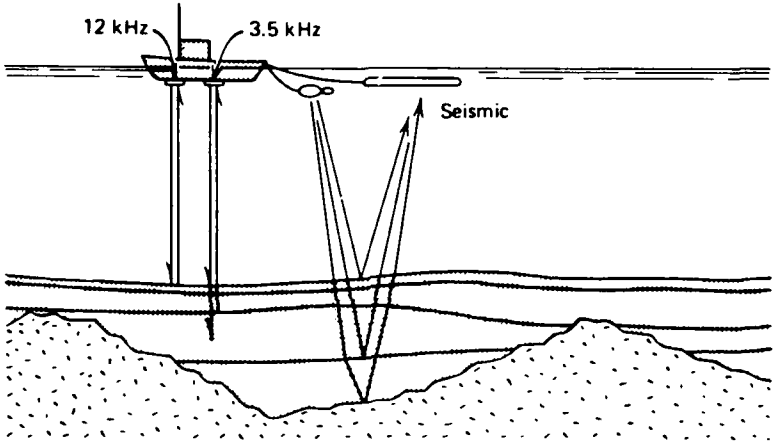

ECHOSOUNDING

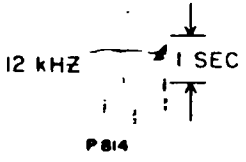

SHALLOW SUBBOTTOM PROFILE

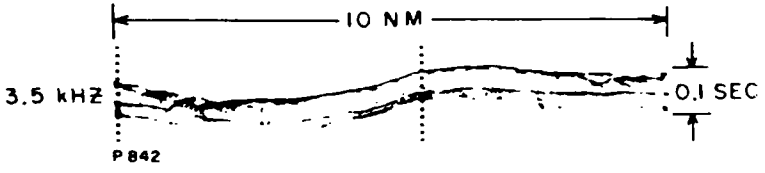

SEISMIC

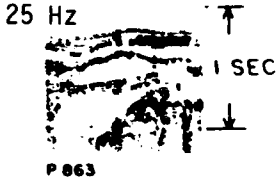

(adapted from Lowrie and Escowitz: 1969)

Figure II-4: Side-Scanning Sonar: Microtopography and Sea Floor Obstructions

An example of the detail achieved by a side-looking sonar of the microtopography and obstructions on the sea floor is shown in this figure (Ref. II-4). It compares a side-scanning sonogram with a chart of the Hudson River near Dobbs Ferry, NY. The location of small features can be determined and monitored relatively quickly by the sonar technique. The sonar was towed about 250 m offshore along the ship's track shown on the chart. The pipeline ditch and sunken barge on the chart are quite visible on the sonogram. For a perfect match the sonogram must be stretched in the north-south direction. Such a device, deeply towed, could be used in classifying a bottomed target such as the Titanic, once it is located by other detection sonar.

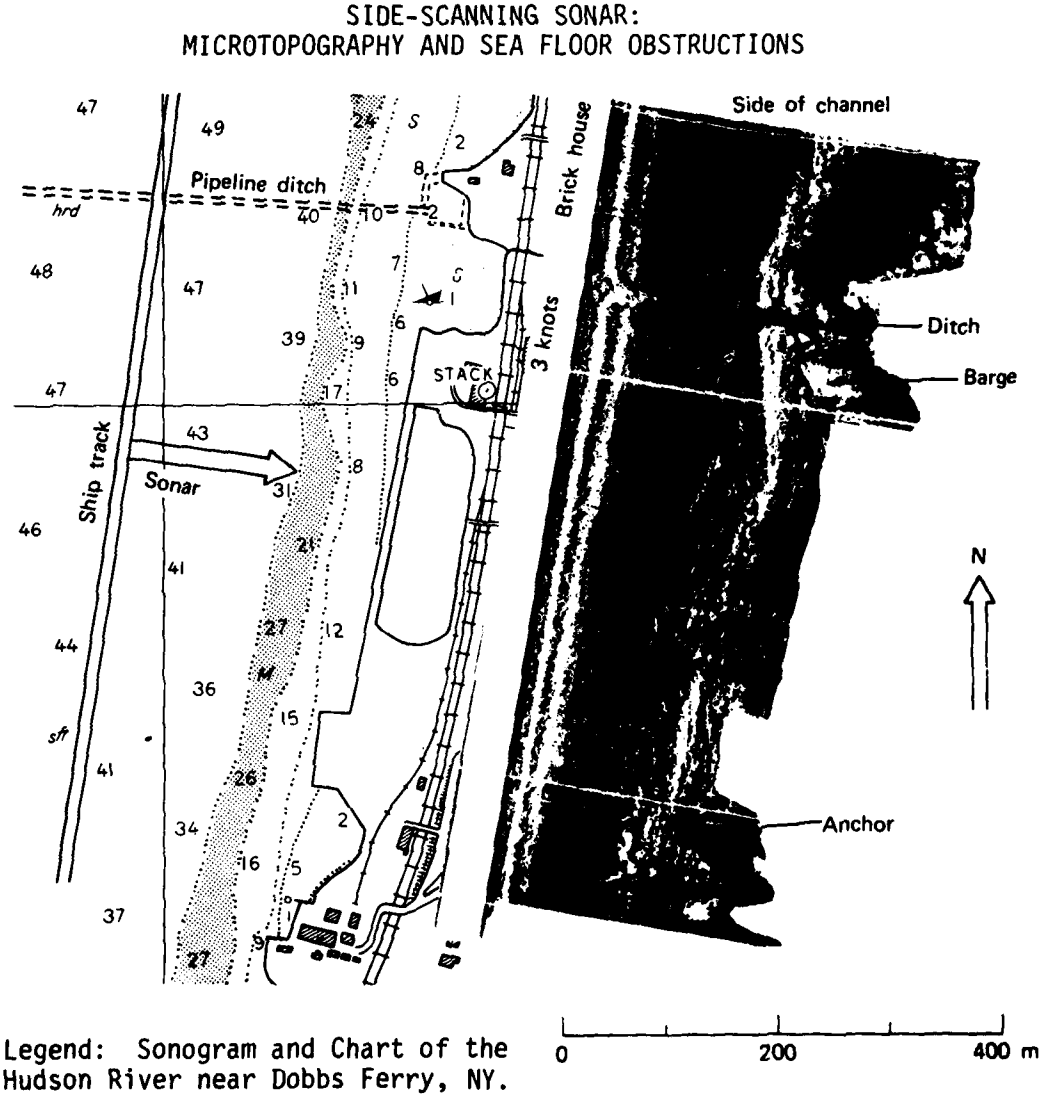

Fig. II-4

Legend: Sonogram and Chart of the Hudson River near Dobbs Ferry, NY.

(Clay and Medwin: 1977)

III. OCEAN CHEMISTRY AND POLLUTION

Figure III-1: Attenuation of Waves in Seawater

This figure compares the attenuation of electromagnetic and acoustical waves in seawater as a function of wavelength. Note that wavelength increases to the left in the figure. At long radio wavelengths the absorption is caused by the conductivity of seawater, 4 mhos/m. In the visible-region window of the figure, the attenuation can vary considerably depending on the particulate content of a specific water mass (Ref. III-1). Acoustical energy propagates with lower absorption ~~below~~ above a wavelength of 1.5 μm. At very high acoustic frequencies there is absorption due to the molecular viscosity of water molecules and much scattering. Acoustic scattering loss is not considered in the plot shown. At about 100 kHz and less there is increased absorption due to the relaxation of the $MgSO_4$ molecule; at about 1 kHz the relaxation of $B(OH)_3$ causes still more absorption. An important property of $B(OH)_3$ absorption is its dependence on pH, a water mass property, which is sensitive to the amount of CO_2 in the ocean (Ref. III-2). Relaxations are acoustic pressure dependent changes of sonic or molecular configurations. Work in progress in ocean chemical acoustics concerns: (1) new relaxations, (2) the effect of high pressure and low temperature on absorption, and (3) the absorption and scattering properties of particulates, suspensoids and pollutants.

Figure III-2: Satellite Remote Sensing -- Coastal Zone Color Scanner (CZCS)

The figure shows another type of information obtained from satellite oceanography (Ref. III-3). It is a scene from the Gulf of Mexico. The CZCS measures the intensity of ocean color in several optical wavelength bands. It can measure ocean sediment load from river runoff and also chlorophyll *a* plus phaeopigments with a resolution of 800 m and swath coverage exceeding 1500 km. Regions of sharp gradients indicate ocean fronts. Mapping these effects enables an in-depth study of their causes and consequences involving biological activities, river runoff and pollution.

Figure III-3: Particulate Density Distributions in the Sea

There is a surprisingly large density of particulate matter suspended in seawater. Particulate matter is defined as the suspended material that is retained by a filter with pore diameter 0.45 μm (sometimes 0.25 μm). In oceanic waters the range is from about 0.05 to 2.0 mg/ℓ, and in coastal waters the range may be from 6 to 18 mg/ℓ. The percentage of organic matter of the total dry weight of suspended material varies from 20 to 60% (Ref. III-4).

The figure shows examples of cumulative distributions on a log scale of the number of particles per cubic meter of seawater vs the log of the particulate diameter in microns. Note that the scale increases to the left. These numbers are usually obtained in vitro by a Coulter counter or microscope. In situ, they are obtained by optical transmissometers and scattering meters. The shapes of the particles may all be different, varying from flakes and needles to irregular grains and spherules. The slope of the curves goes roughly as the -3 power of diameter. In the measurements by Proni et al. (Ref. III-5) the distributions of particle sizes within and below the sediment dredge cloud are different below a diameter of 7.8 μm. As will be seen later, the acoustic backscattering from contiguous layers enables the measurement of current vs depth profiles using doppler shifts in frequency.

Figure III-4: Ocean Pollution Acoustics

Acoustical techniques have been found useful in the measurement and monitoring of various types of ocean pollution. Functions that have been performed are: reconnaissance, mapping, seawater sampling design and time-series observations. Some of the subjects studied are: waste disposal (municipal and industrial); dredging operations, outer continental shelf development, hazardous material (including oil) spills, resource mining and energy utilization.

Proni et al. (Ref. III-5) have used two towed systems at 20 kHz and 200 kHz simultaneously to study the backscattering properties of sewage sludge dumped in the ocean. These systems were towed at a depth of 2 m on opposite sides of the ship. In the figure we see that after 1 hour sludge was no longer directly detectable at 20 kHz; although it was indirectly detectable through point scatterers. The 200 kHz system was still detecting sludge directly after 4 hours. Backscattering from biological layers was also observed and the depth of the mixed layer could be delineated.

Figure III-5: Acoustic Scattering of a Bubble and Small Solid Sphere

Distinguishing among the scattering properties of bubbles, suspensoids, particulates, and ocean finestructure and microstructure density patches has become of great importance because the same acoustical backscattering techniques are used to study these ocean properties. The present figure compares the basic differences in the scattering properties of bubbles and solid spheres (Ref. III-6). It can be seen that the scattering cross section of a bubble is about 1000 times its actual cross section at a circumference to wavelength ratio of 1/100. The scattering cross section of a solid sphere approaches its geometrical cross section. Both types of objects have a Rayleigh scattering region with a rapid rise in scattering for small object size compared with the wavelength. However, in its Rayleigh region, the bubble has to be only 1/100 the size of the solid sphere to produce the same scattering.

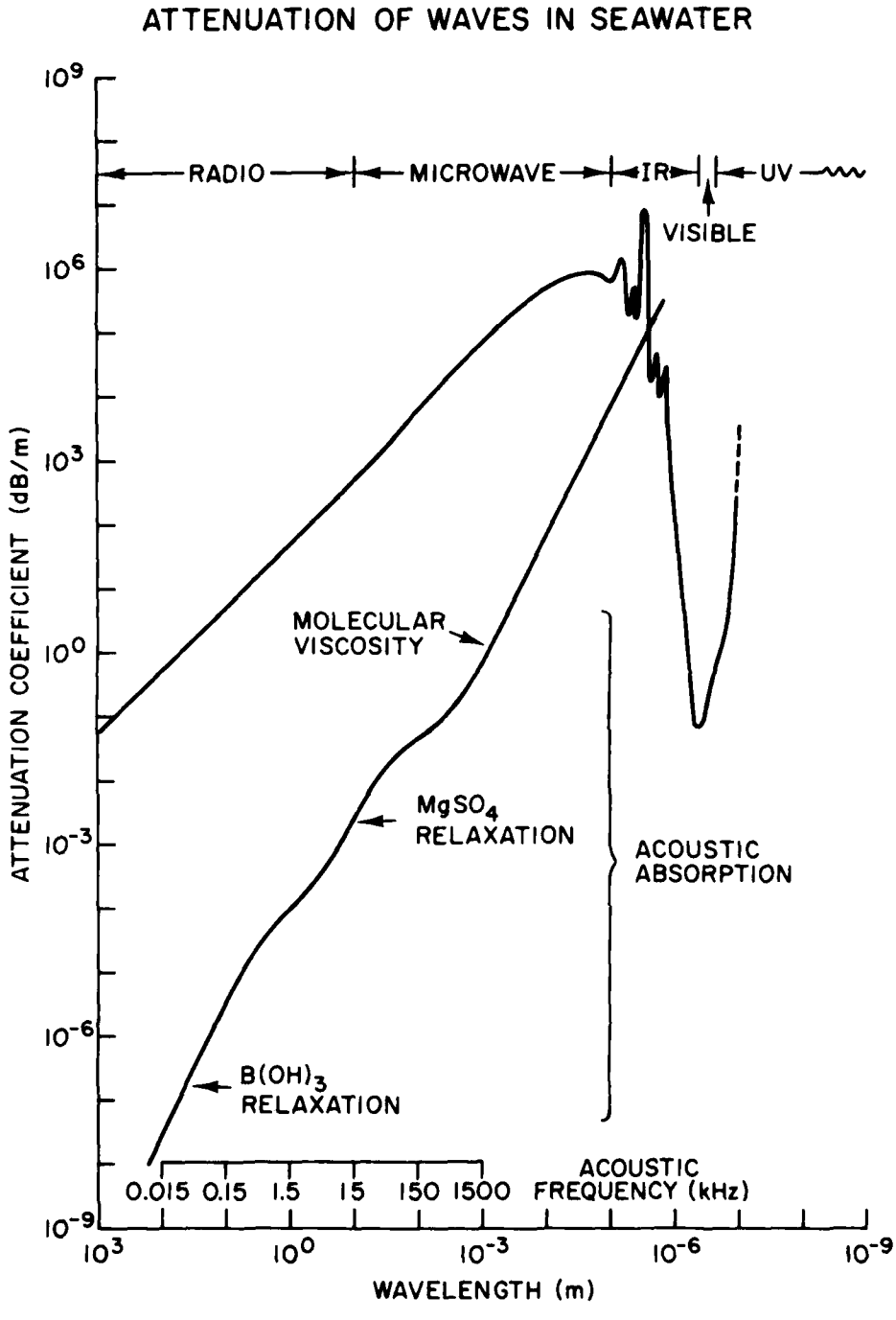
ATTENUATION OF WAVES IN SEAWATER
RADIO
MICROWAVE
IR
UV
VISIBLE
ATTENUATION COEFFICIENT (dB/m)
MOLECULAR VISCOSITY
MgSO4 RELAXATION
B(OH)3 RELAXATION
ACOUSTIC ABSORPTION
0.015 0.15 1.5 15 150 1500
ACOUSTIC FREQUENCY (kHz)
WAVELENGTH (m)

Fig. III-1

SATELLITE REMOTE SENSING -- COASTAL ZONE COLOR SCANNER (CZCS)

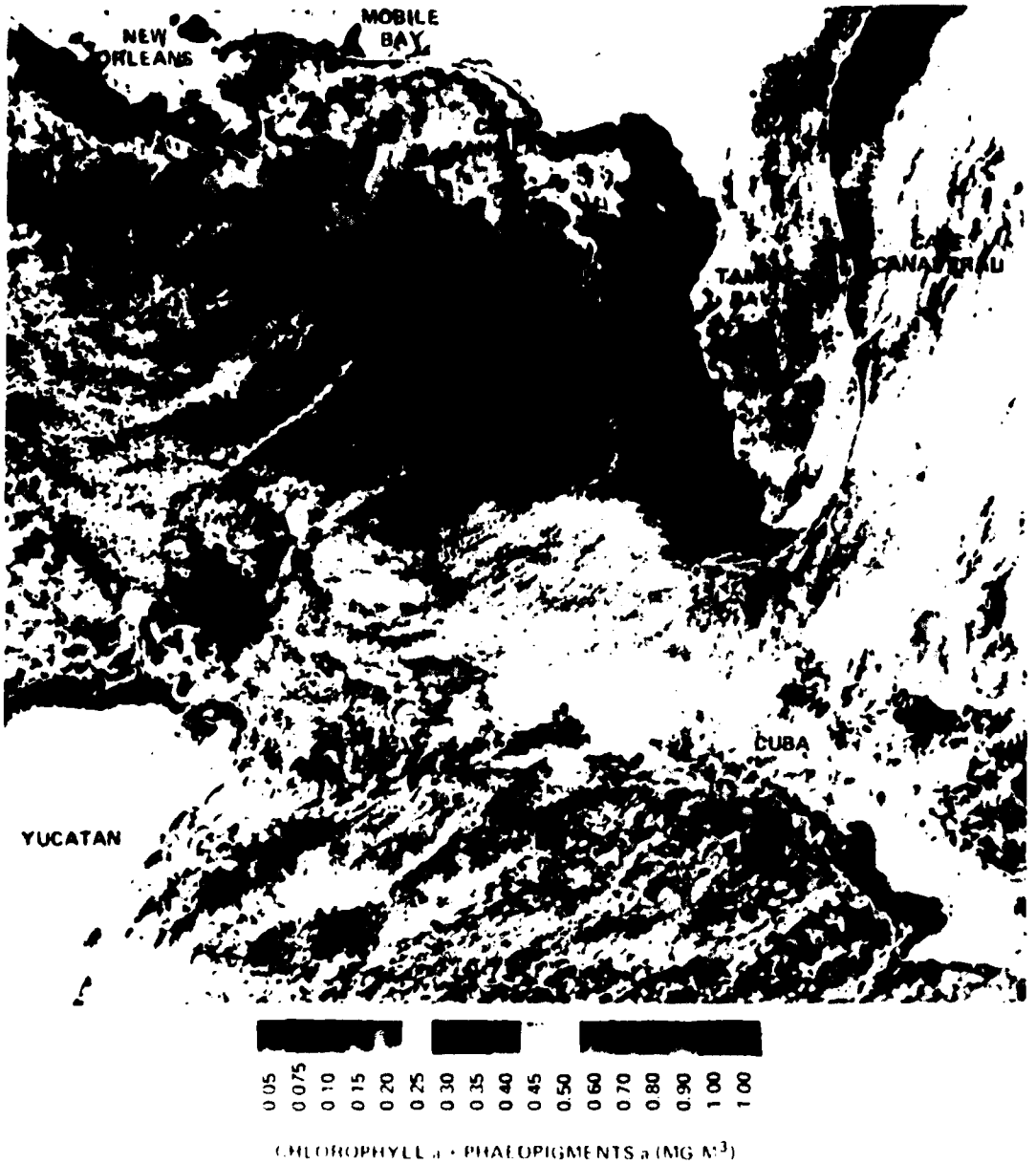

Fig. III-2

(N. Anderson: 1980)

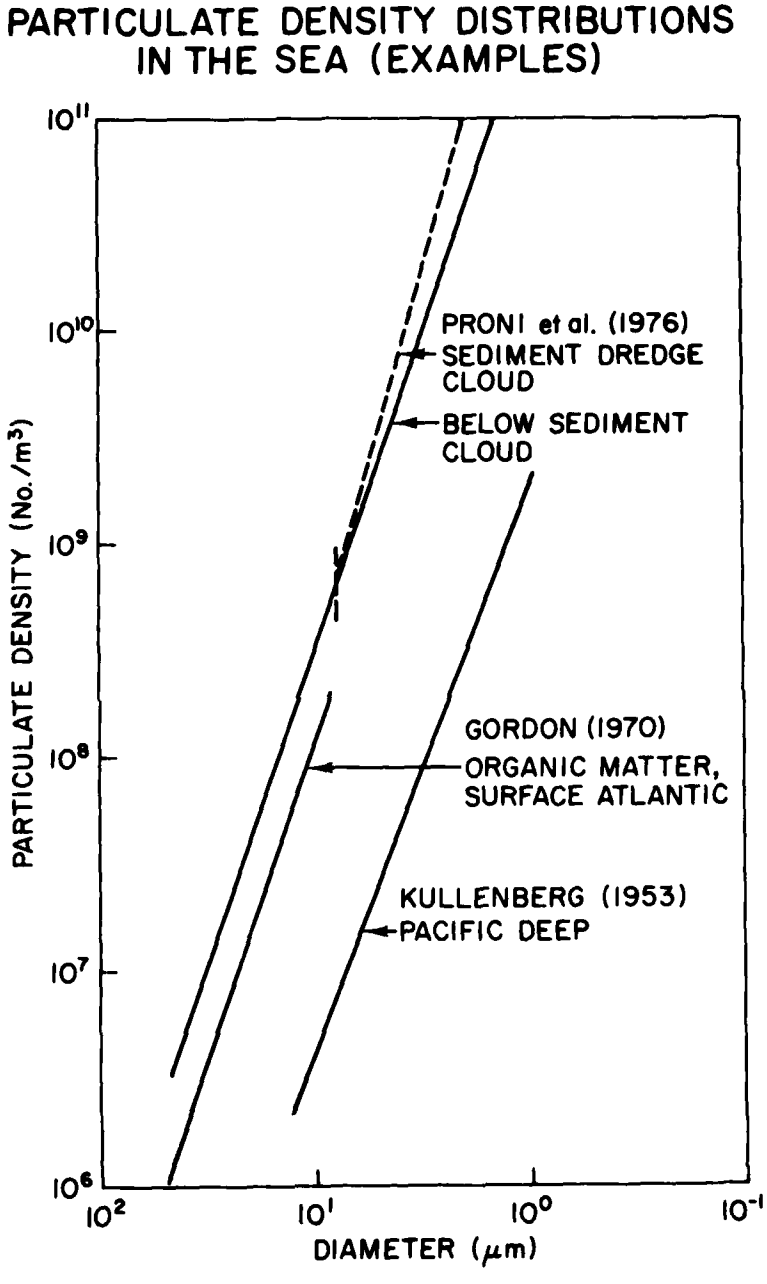
PARTICULATE DENSITY DISTRIBUTIONS
IN THE SEA (EXAMPLES)
PARTICULATE DENSITY (No./m³)
10¹¹
10¹⁰
10⁹
10⁸
10⁷
10⁶
PRONI et al. (1976)
SEDIMENT DREDGE CLOUD
BELOW SEDIMENT CLOUD
GORDON (1970)
ORGANIC MATTER, SURFACE ATLANTIC
KULLENBERG (1953)
PACIFIC DEEP
10²
10¹
10⁰
10⁻¹
DIAMETER (μm)

Fig.
III-3

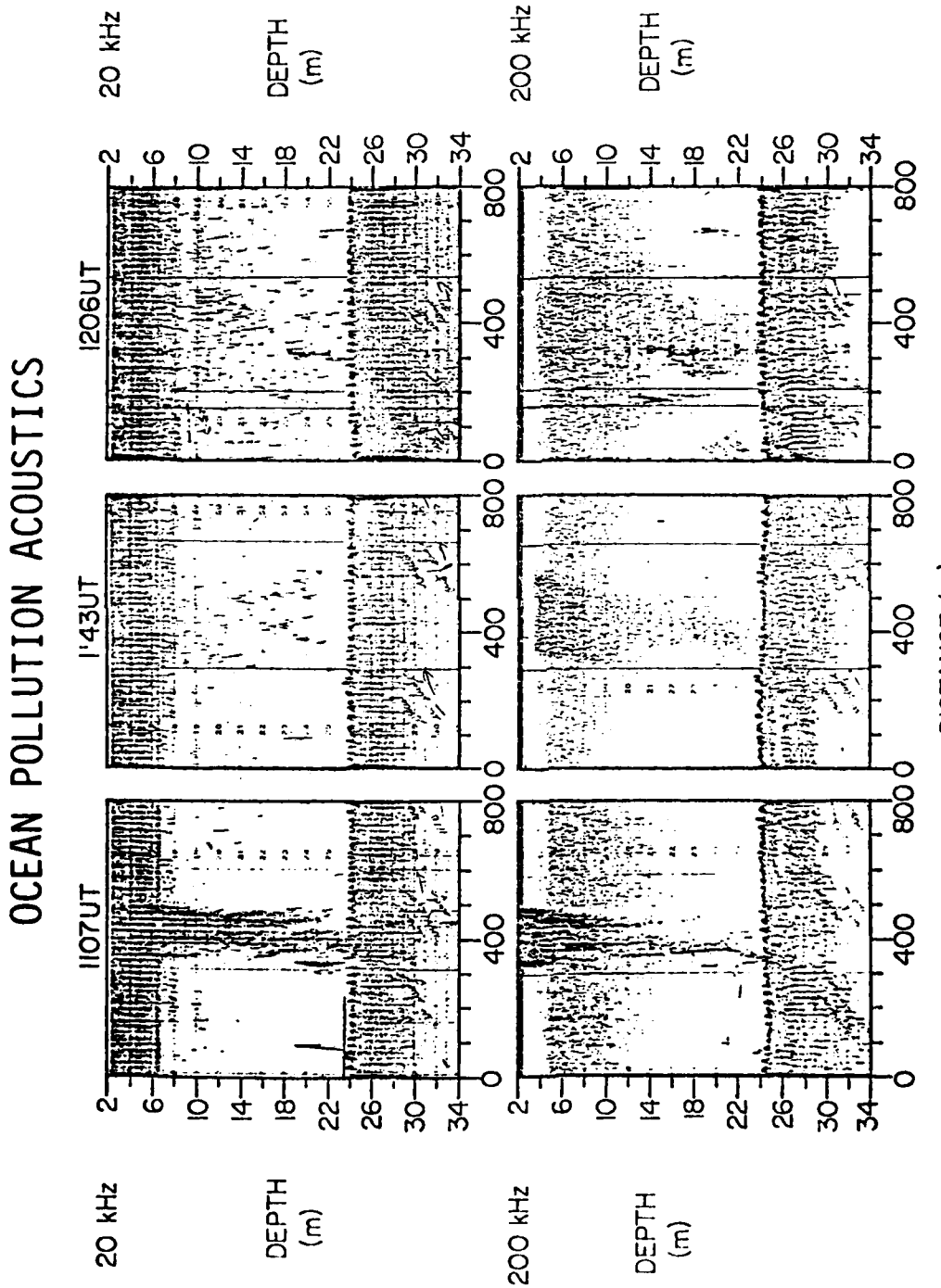
OCEAN POLLUTION ACOUSTICS
1107UT
1143UT
1206UT
20 kHz
200 kHz
DEPTH (m)
DISTANCE (m)
SLUDGE TRACKING EXPERIMENT STAX
SEPTEMBER 22, 1975
(Proni et al.: 1976)

Fig. III-4

ACOUSTIC SCATTERING OF A BUBBLE AND SMALL SOLID SPHERE

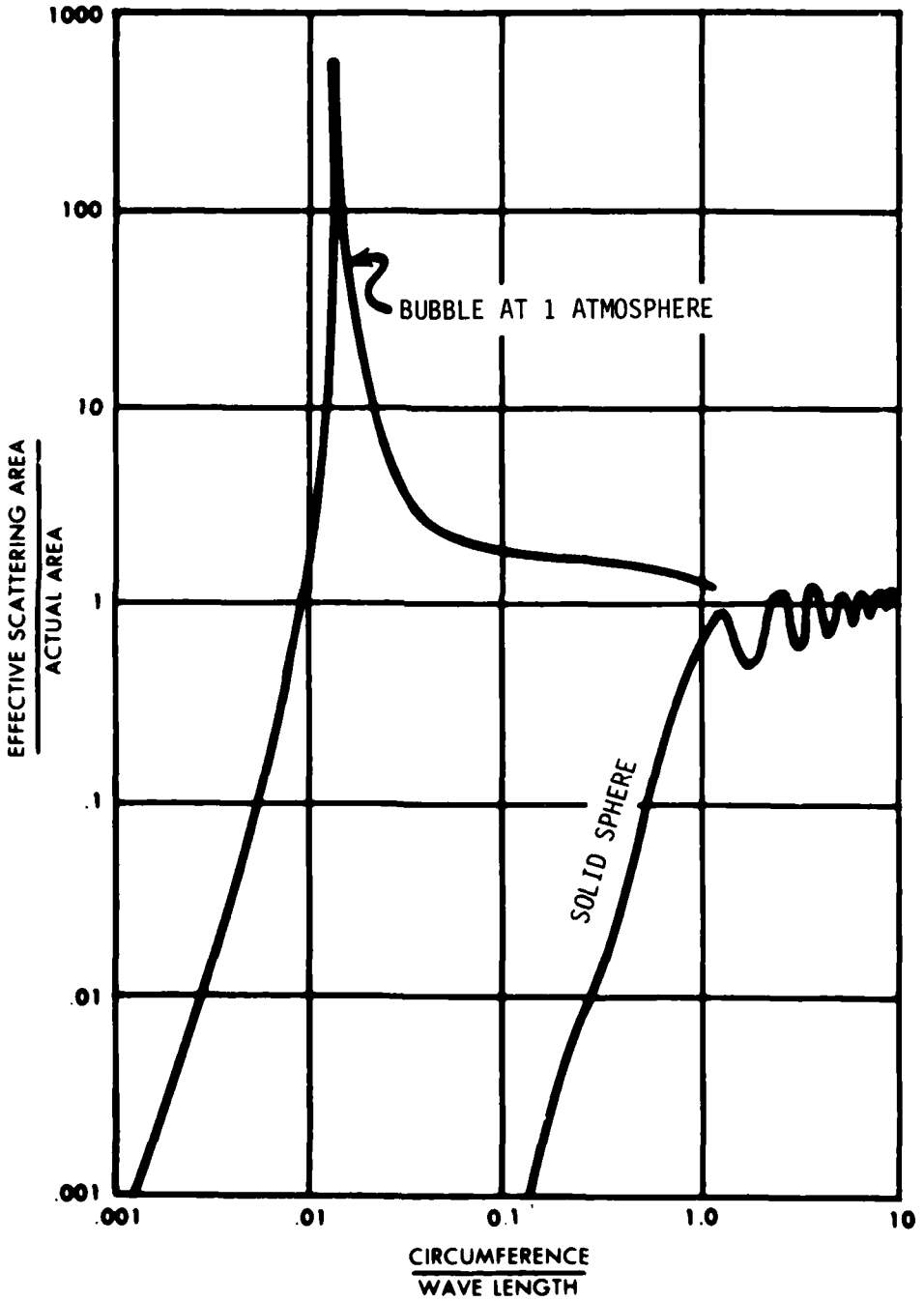

Fig. III-5

(NAVOCEANO: 1966)

IV. BIOMASS AND FISHERIES

Figure IV-1: Scattering Cross Section of Individual Bladder Fish

Many fish have swim bladders that behave like bubbles for acoustic scattering. The swim bladder has a volume of from 5 to 7% of the total fish volume. There is, however, considerable damping introduced by fish tissue, thus broadening and lowering the resonance peak. The combined bubble and solid body scattering cross section of a single swim bladder fish is shown in the figure as a function of the ratio of length to wavelength (Ref. IV-1, 3).

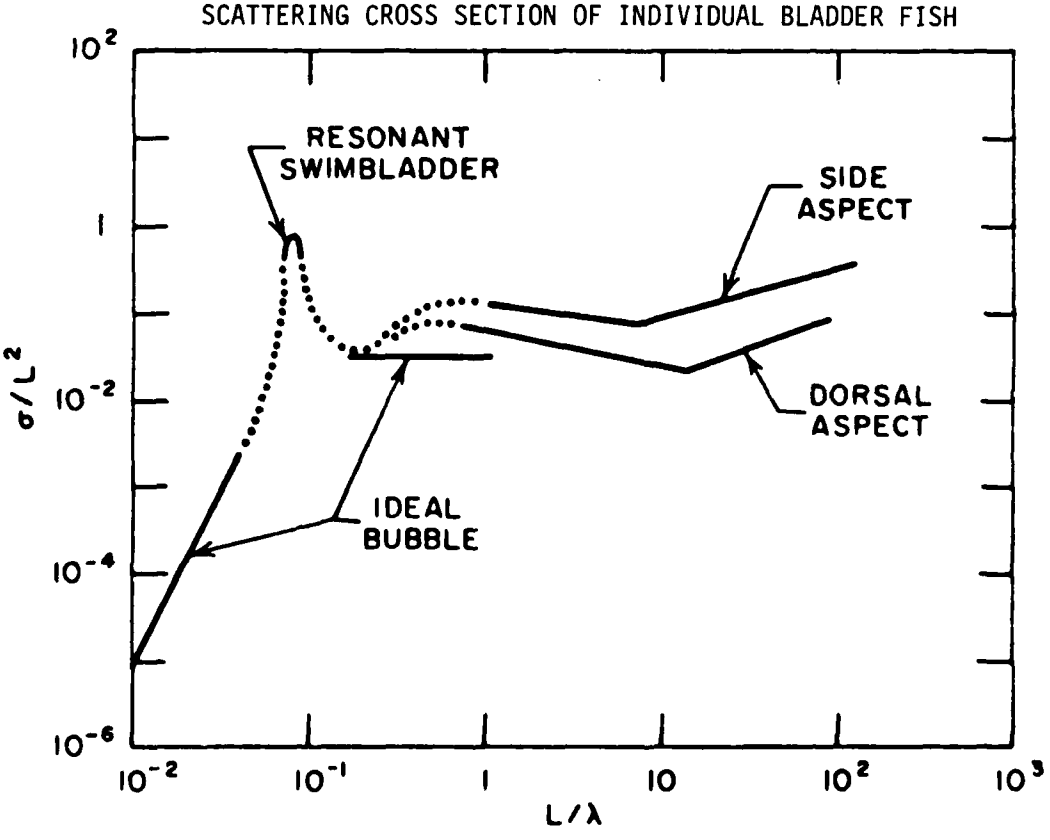

Fig. IV-1

(Love, Winokur, Levenson: 1974)

Figure IV-2: The Deep Scattering Layer (DSL)

The phenomenon of the deep scattering layer (DSL) is shown in the figure (Ref. IV-2). The acoustical properties of the DSL were discovered using depth sounders. In this figure the data were obtained at 30 kHz. The scattering layers are light-sensitive ecological systems involving plankton and swim bladder fish. The DSL exhibits a diurnal rise toward the sea surface after sunset and a descent to depth after sunrise.

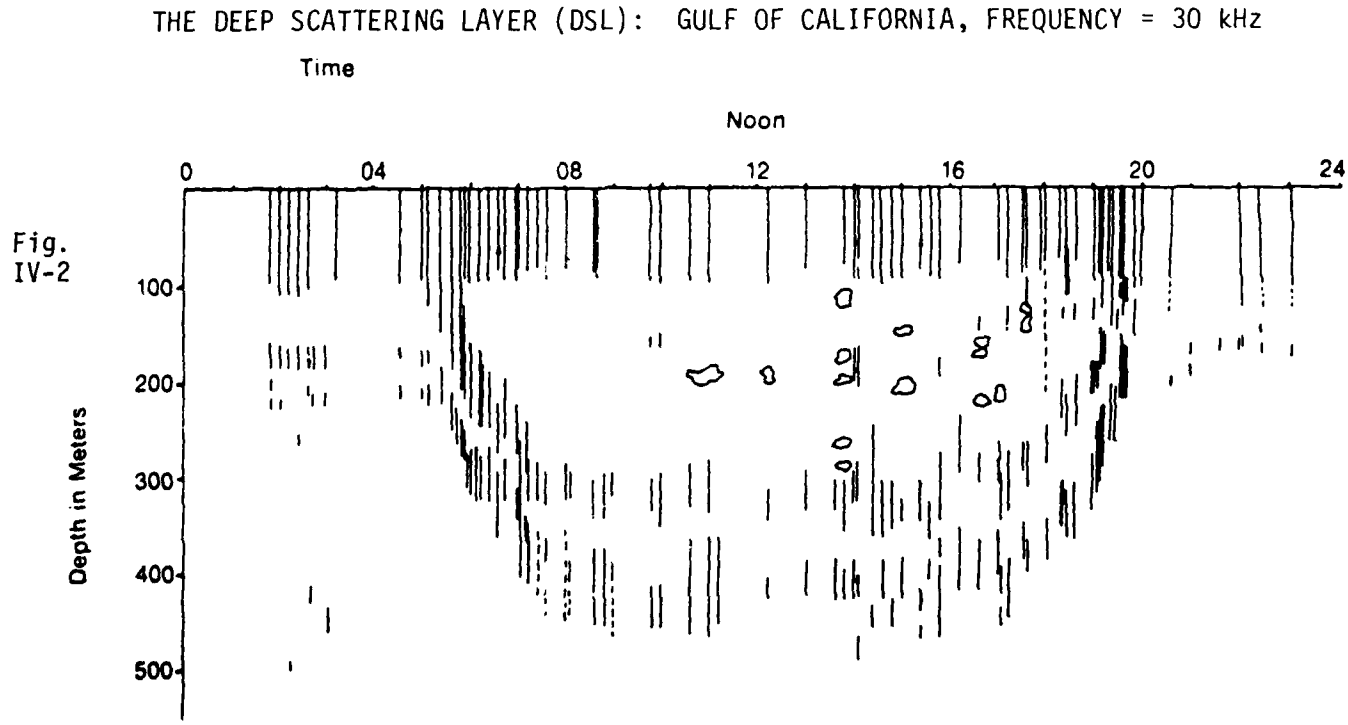

Fig. IV-2

(Dunlap: 1970)

Figure IV-3: Scattering Layer Reconnaissance (Mediterranean)

Prior to the application of detailed acoustical studies, some form of reconnaissance is useful. An aircraft reconnaissance technique developed by the Navy is to use 1.8 lb charges exploded at 60 m depth for broadband frequency coverage, and sonobuoys for detecting the reverberation out to 800 m range and 800 m depth. Column scattering strength is then obtained as a function of range and acoustic frequency. In the figure, we show the nature of the acoustical frequency dependence of the scattering as a function of diurnal and seasonal effects in the Mediterranean as measured by column scattering strengths. These are the scattering measures obtained by using explosive charges to cover relatively large volumes of the ocean. Note that winter night and summer day have the highest and lowest returns respectively.

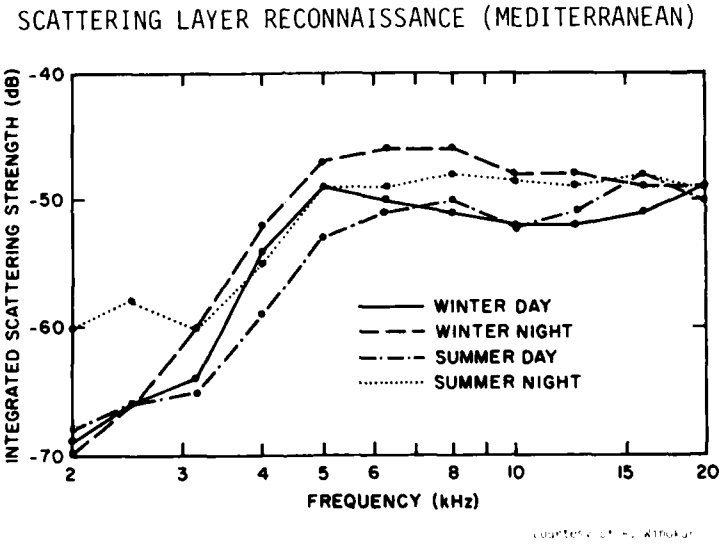

Fig. IV-3

Figure IV-4: Echograms of Fish Schools

The echosounder is the most common device used for locating fish schools for fishery stock assessment, as well as fishing. The echosounder may be towed or hull-mounted. Fishermen use the display to locate fish aggregations, judge species composition, estimate biomass and plan fishing tactics. The fisherman relies on past experience based on knowledge of the area and of the schooling characteristics of target species to make subjective evaluations. The figure shows three examples of echograms of fish aggregations (Ref. IV-3). Such echograms are a form of sonar mapping.

ECHOGRAMS OF FISH SCHOOLS

SCHOOLS

SINGLE FISH AND SMALL SCHOOLS

MIXED SCHOOLS

Fig.
IV-4

(Love, Winokur, Levenson: 1974)

Figure IV-5: Acoustical Techniques for Fishery Stock Assessment (Ref. IV-4)

- ECHO COUNTING
- ECHO INTEGRATION
- SONAR MAPPING

Fig. IV-5

1. Echo counting--narrow beam transmitters and receivers are used for resolving and counting echoes from individual fish. In situ target strengths can be measured for individual fish.

2. Echo integration--echoes from fish schools are integrated for abundance estimates. It is possible to obtain in situ target strengths for fish aggregates.

3. Sonar mapping--at present sonar mapping is the best developed form for the assessment of pelagic schooling fish stocks. The dimensions of the fish school are obtained from the sonar features of ranging, pulse timing and beam width. In addition, resonance frequency analysis of returns is used to infer fish species and size. Doppler frequency shift can be used to measure tailbeat which together with school speed gives an estimate of fish length.

Figure IV-6: Sonar Mapping of Fish Schools

The figure shows how the incoherent target strength of a fish school depends on the value for a single fish in terms of sonar and geometrical parameters (Ref. IV-5). Using doppler sonar, fish school speed with respect to the ship can be obtained along with tailbeat frequency data, from which the average size of an individual fish in the school can be derived (Ref. IV-6). For specific data interpretation, direct fish sampling surveys (net hauls) are needed to supplement the sonar information. Sonar systems are also being used for counting and assessing fish stocks in restricted places such as streams and lakes.

SONAR MAPPING OF FISH SCHOOLS

A. Target Strength (Incoherent) of Fish School

$$TS = TS_i + 10 \log D + 10 \log V' - A \quad \text{dB}$$

TS is school target strength (incoherent component)

TS_i is individual school member target strength

D is schooling density in fish/m^3

V' is volume of school sampled by sound cone

Fig. IV-6

A is attenuation due to school scattering and absorption

B. Fish Speed vs Length and Tailbeat (Bainbridge's Relation)

$$v = \frac{L}{4}(3F - 4) \quad \text{m/s}$$

v = swimming speed (m/s)

L = body length (m)

F = tailbeat frequency (Hz)

V. OCEAN DYNAMICS -- MACROSCALE, SYNOPTIC SCALE AND MESOSCALE

Figure V-1: Sketch of Kinetic Energy Spectrum and Scales of Motion

In this figure, a sketch is given of the kinetic energy spectrum and scales of motion in the ocean (Ref. V-1). The basic source of energy is the sun. The scale name and associated acoustic probe frequency are merely indicative and not definitive. The peaks are zones of kinetic energy input and are separated by zones of the 5/3 law of dissipation. The macroscale is the size of ocean basins and gyres, 5000 to 1000 km, and has time variations of the order of decades to seasonal. The synoptic scale is of the order of 1000 km and refers to the energy input of atmospheric high and low pressure areas associated with weather. The mesoscale region is the region of major currents, meanders, upwelling, fronts, and warm and cold ring eddies. Time variations here are a few months to a few days. Inertial motions refer to the effect of the earth's rotation on currents. This region is followed by a region of dissipation occupied by internal waves, internal tides and their associated currents. Time variations associated with this region are fortnightly to tens of minutes. Next is the scale of local wind waves. Time variations associated with this scale are daily to a few minutes. Inside the ocean we have finestructure on this length and time scale. The breakdown of finestructure leads to microstructure with lengths less than a half meter and time changes of less than a few minutes.

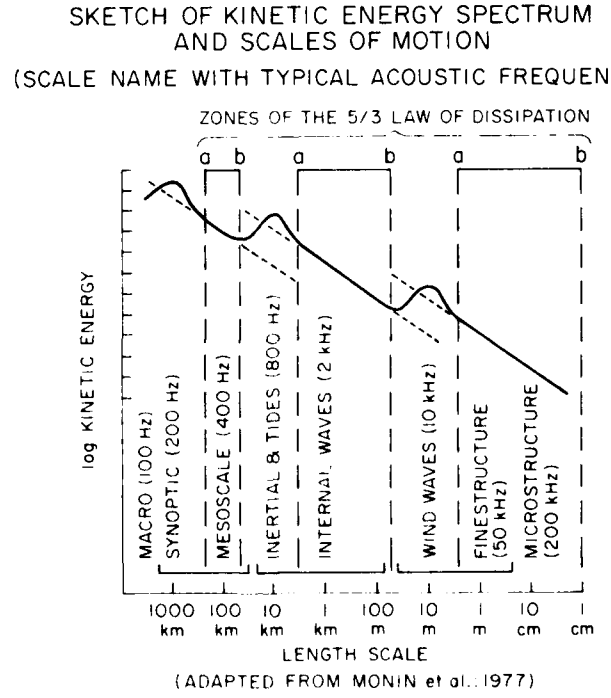

Fig. V-1

Figure V-2: Satellite Mesoscale Resolution

In addition to satellite ocean surface topography and color scanning maps, maps of mesoscale temperature features can be obtained by eliminating cloud "noise" of less than 7 days duration. The map shown was devised by A.E. Pressman and J.R. Clark of NORDA, and shows the Gulf Stream, a meander and ring eddies on a latitude-longitude scale about 2000 km on a side. It was obtained by processing GOES satellite data obtained three times a day for 7 consecutive days. The warmest temperature of these 21 values is plotted for each 10 km x 10 km pixcel. The color scale of temperature is shown at the top of the map. Smearing occurs if one makes the sampling period too long. A motion picture is then made of consecutive frames showing the development and decay of surface mesoscale features. These features can be further investigated in depth by using ocean acoustic remote sensing systems.

SATELLITE MESOSCALE RESOLUTION

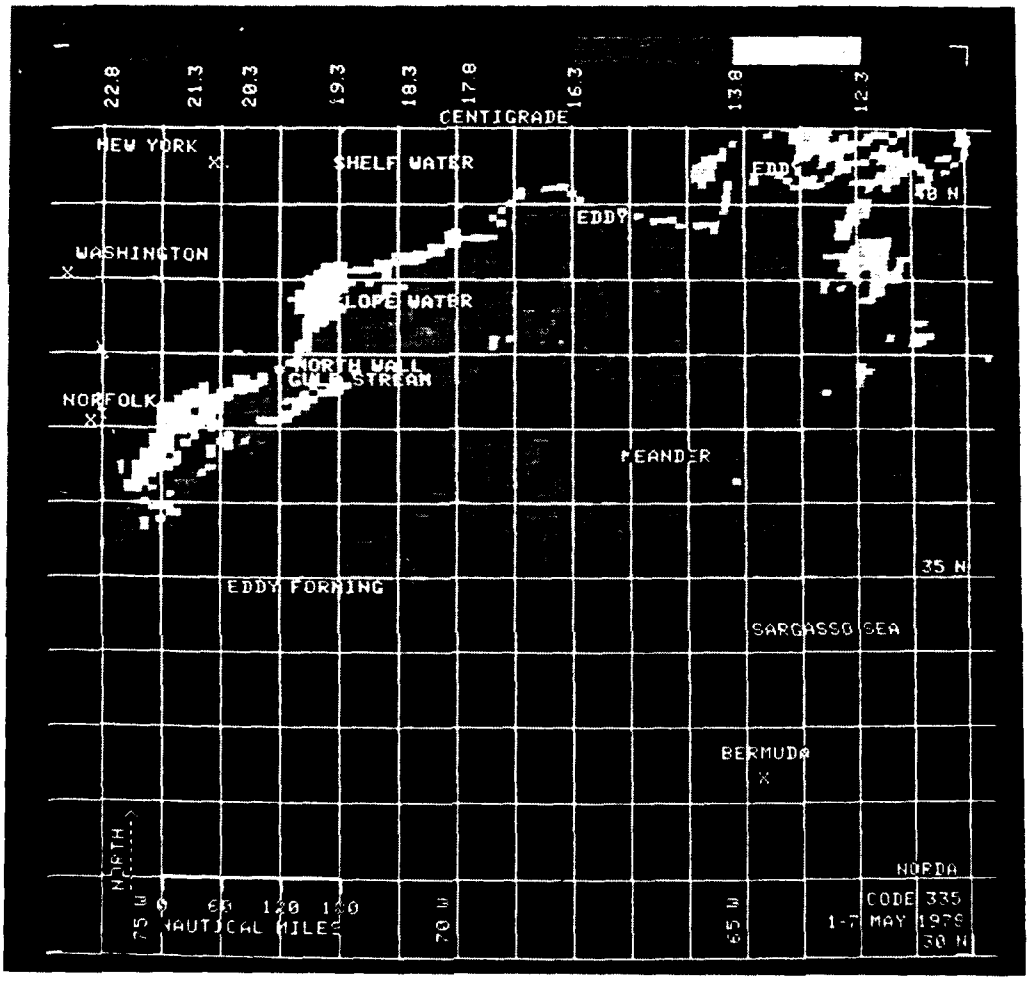

Fig. V-2

(Originally in color)

(Courtesy of A.E. Pressman and J.R. Clark)

Figure V-3: Mesoscale Variability -- Acoustic Propagation Loss

Time variability over a mesoscale path of fixed length and acoustic frequency should reflect ocean mesoscale time periods. In the figure (Ref. V-2), a set of transmission loss variability data is shown for the 1260 km path between Eleuthera and Bermuda. Two-day means of transmission loss data taken over a 5 month period show a 20 dB excursion. Peaks drop to minima in about 20 days here. There is about a 7 dB standard deviation. Acoustic changes in phase (travel time here is about 14 minutes) and amplitude are expected to depend on changes in currents and temperature.

Figure V-4: Ocean Acoustic Tomography

By using arrays of fixed transmitters and receivers, the concept of ocean tomography has been proposed to monitor mesoscale temperature and current changes by inverting the measured changes in travel times (i.e., sound speed) for identifiably-coded acoustic rays. One-way changes can yield the temperature field. Reciprocal path transmissions are required for current determination. The figure shows a horizontal slice of a tomographic array configuration proposed by Munk and his coworkers for a region of the North Atlantic (Refs. V-3, 4). On the left, the acoustic travel time is measured along the 16 paths between four sources and four receivers covering a 1000 km x 1000 km region. The right side shows, for assumed departures in sound speed for 16 subareas, the corresponding values obtained by inversion of travel time departures for two error conditions, 0 sec rms and 0.1 sec rms.

Fig. V-3

MESOSCALE VARIABILITY -- ACOUSTIC PROPAGATION LOSS

Eleuthera to Bermuda Path (1260 km)

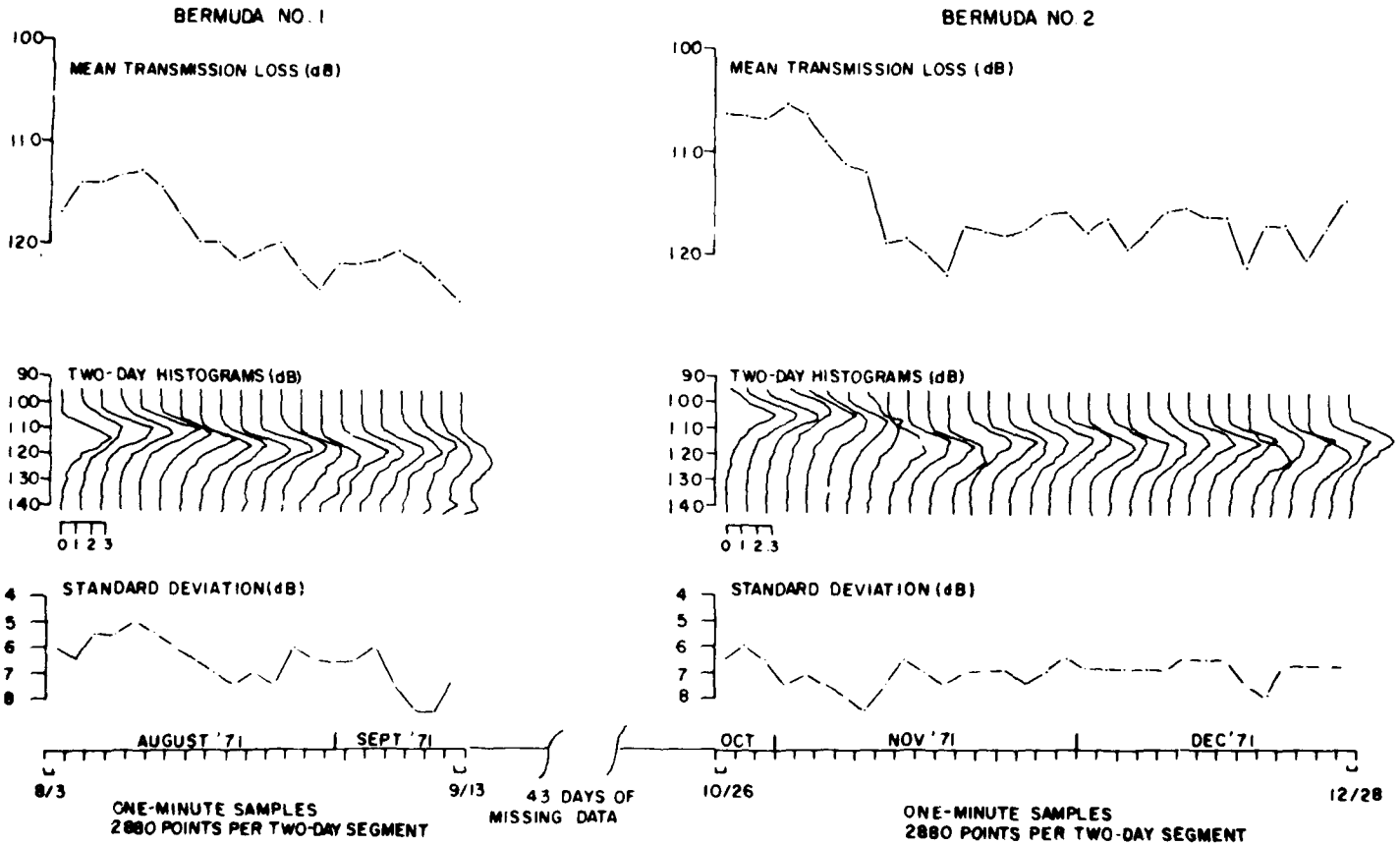

(Clark and Kronengold: 1974)

OCEAN ACOUSTIC TOMOGRAPHY

Tomographic Array (Proposed) -- Horizontal Slice

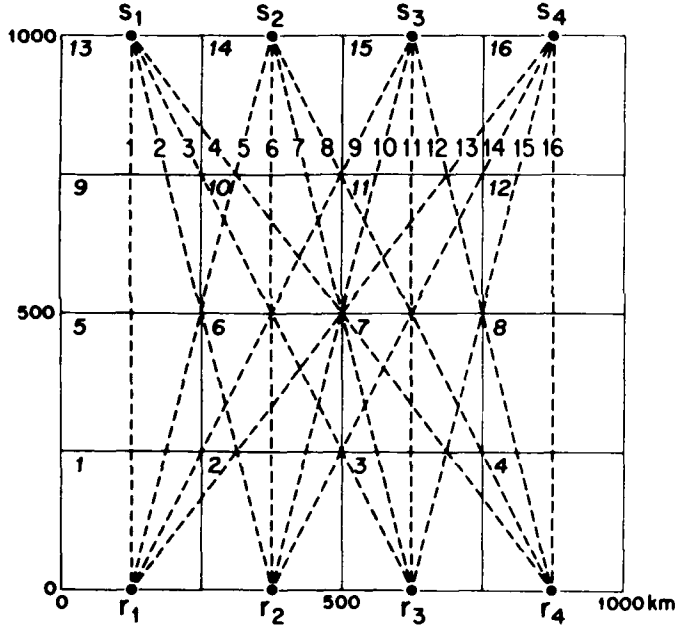

Area: 1000 km x 1000 km with 16 subareas

2. 1.1 0.7	-2. -1.9 -1.6	2. 3.0 4.2	-4. -2.0 -2.5
-1. 0.3 2.0	-1. -0.7 -1.1	5. 4.3 3.3	-2. -3.6 -3.4
1. 0.5 -0.1	2. 0.5 0.4	3. 0.6 0.9	2. -1.4 -0.4
4. 4.1 3.8	-4. -2.9 -2.3	-4. -1.9 -1.5	-2. 1.0 0.7

0 500 1000km

Departures in sound speed, m s^{-1}

(Munk: 1980)

Fig. V-4

VI. OCEAN DYNAMICS -- INTERNAL WAVES AND TIDES

Figure VI-1: Temperature Power Spectrum of Internal Waves and Tides

A square law of turbulent decay in energy occurs in the progressive internal wave region which lies between the inertial frequency and the buoyancy frequency. A measured moored-temperature variance spectrum showing this behavior is plotted for such frequencies at Cobb Seamount off the coast of Oregon at a depth of 1203 m. Tidal peaks occur at 8.3 x 10^{-2} h^{-1} (12 hours) and 4.2 x 10^{-2} h^{-1} (24 hours) (Ref. VI-2).

Fig. VI-1

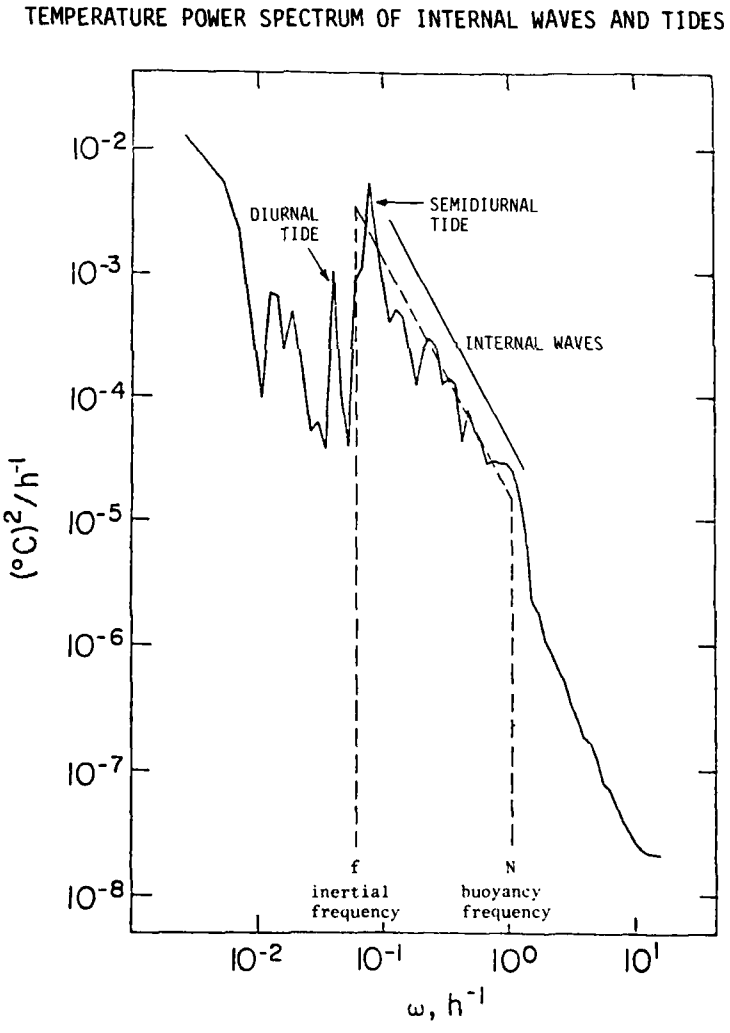

(Levine: 1979)

Figure VI-2: Acoustic Phase Power Spectrum of Internal Waves

Many acoustical measurements have been made of internal wave effects. In this figure, the spectrum of acoustical travel time variability is plotted against internal wave frequency in hertz for a 17.2 km path between Cobb Seamount and a neighboring seamount. A frequency of 4 kHz was used. Note the good agreement between the measured and theoretical spectra.

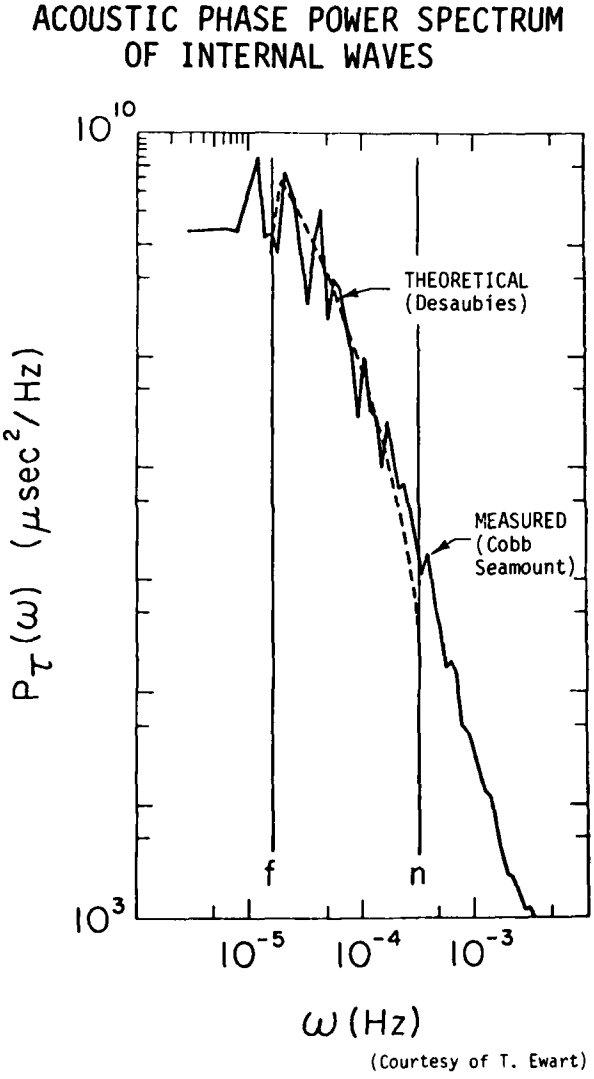

(Courtesy of T. Ewart)

Fig. VI-2

VII. OCEAN DYNAMICS -- SEA SURFACE AND NEAR-SURFACE LAYER

Figure VII-1: Inverted Echosounder (IES)

Surface wave height can be monitored by using an inverted echosounder (IES) mounted at the bottom (Refs. VII-1, 2, 3). The IES measures the travel time to the surface and back. Because changes in the depth of the thermocline are much greater than changes in the surface wave height and have a longer time period, it is possible to distinguish between the two. Also, tidal height changes can be eliminated through their periodicities. Using a two-layer ocean model and identifying the depth of the thermocline as corresponding to the depth of a particular isotherm for a particular time and location, it is possible to monitor changes in the depth of the thermocline. This enables one to determine the mean heat content of the water column, and consequently the total heat transport when water flow data are also available.

The figure shows the sort of agreement that is obtained between the derived depth of the 15°C isotherm and the depth observed with a temperature device. The rms error of 17.7 m is small compared with the thermocline excursion between 100 m and 700 m. An array of IES's can also be used to monitor Gulf Stream meanders and the depth profile of warm and cold core eddies.

Figure VII-2: Weather Observation Through Ambient Noise (WOTAN)

A bottom-mounted receiver of an inverted echosounder system can be used to monitor ambient noise arriving from the sea surface (Refs. VII-3, 4). This makes it possible to determine the wind speed and wind stress on the surface. The noise intensity increases roughly as the square of the wind speed, i.e., the spectral level increases about 7.2 dB/wind speed doubled. In the figure is shown the wind speed as determined through ambient noise (WOTAN) measurements at 14.5 kHz compared with that measured by a vector averaging wind recorder (VAWR). The ambient noise measurements were made at three frequencies: (1) 14.5 kHz monitoring the sea surface to 6 km radius; (2) 8 kHz monitoring the sea surface to 12 km radius; and (3) 4.3 kHz monitoring the sea surface to 16 km radius. The use of three frequencies simultaneously can also give information on the dominant noise mechanism. For example, the noise level due to the wind stress has a red spectrum while that due to rain has a white spectrum.

INVERTED ECHOSOUNDER (IES)

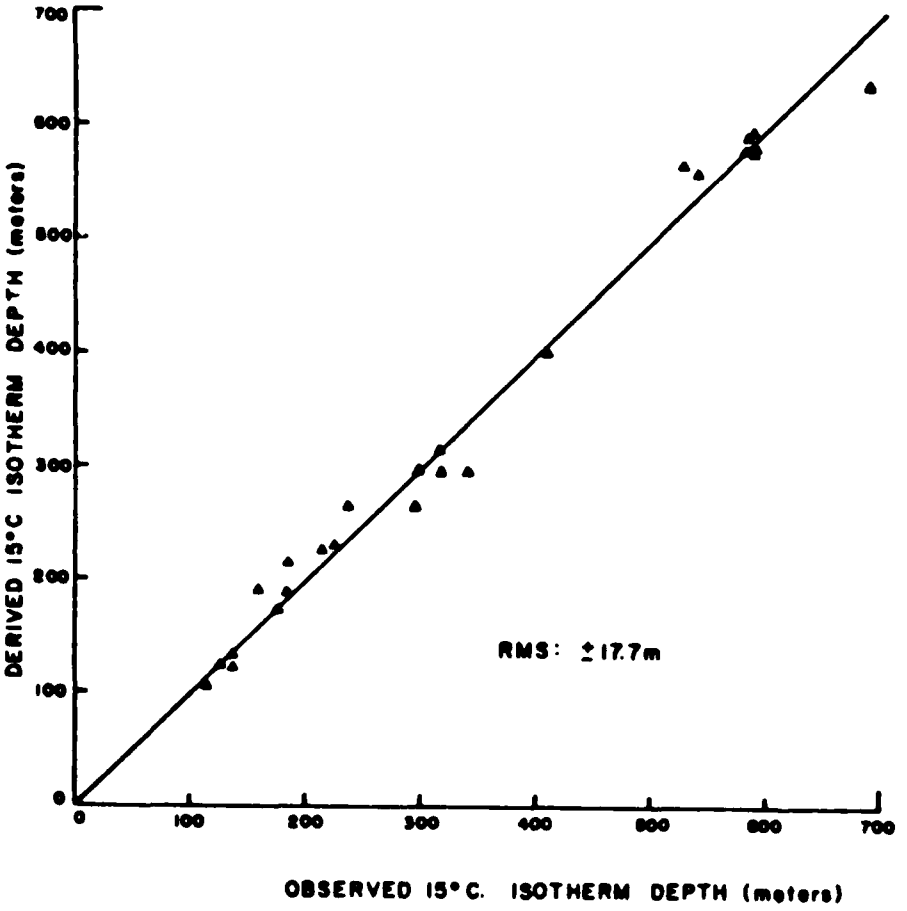

Fig. VII-1

(Bitterman and Watts: 1979)

WEATHER OBSERVATION THROUGH AMBIENT NOISE (WOTAN) -- 14.5 kHz WOTAN WIND CORRELATION

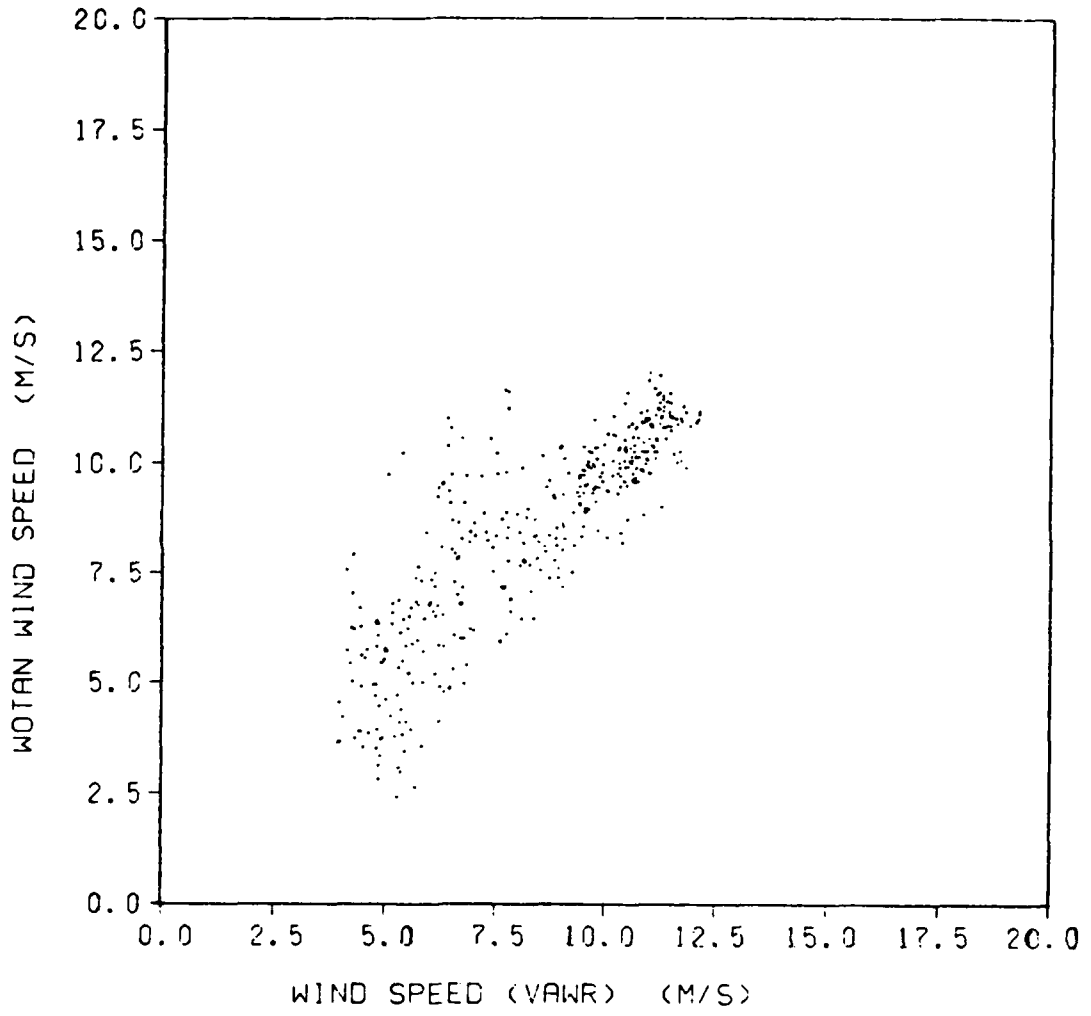

Fig. VII-2

(Watts: 1980)

Figure VII-3: Directional Wave Spectrum of the Sea Surface

Roderick (Ref. VII-6) has measured the directional wave spectrum of the sea surface in shallow water using a horizontal line array of five IES sensors. The sensors simultaneously measured the time-varying wave height at five discrete points on the sea surface. The IES operated at 450 kHz with 16 μs pulses from a tower at 3 m below the surface. The minimum spacing between the sensors was 30 cm; the maximum spacing was 270 cm. The transition region from the near to far field of the transducers produced a spot size on the surface smaller than the 4 cm diameters of the circular piston transducers. Visual observations of the sea surface and wind direction measurements were used to resolve the front to back ambiguity of the array.

The upper part of the figure shows the one-dimensional wave height spectrum obtained by one sensor as compared with the Pierson-Moskowitz model for wind speeds of 4.0 and 5.1 m/s, the range of the observed wind speeds. The dots are the measured data and show a 10 s swell (0.1 Hz). The bottom part of the figure shows the normalized directional wave spectra for the swell and the peak surface wave frequency at 0.267 Hz. The directions and spectral shapes of each component are different. The directional resolution of the method is brought out by the fact that the wavelength of the swell is almost 60 times that of the array length and that of the peak frequency is 8 times that of the array.

Figure VII-4: Vertical Profile of the Horizontal Current Field

There are several acoustical techniques under development, including doppler (Refs. VII-7, 8) and correlation (Ref. VII-9), for measuring vertical profiles of the horizontal current field. These techniques measure the relative motion of contiguous scattering layers as a function of depth and referred to the bottom. In the particular case shown, doppler shifts are measured by echo-ranging transducers which are ship-mounted in the so-called JANUS configuration (four beams, two looking forward and two backward). This method is a natural extension of the ship velocity measurement system. The motion of the ship must be considered in deriving the current shear data. Other possible platforms for current measurements are buoys and bottom mounts. The figure shows the large changes in current direction and magnitude that exist with respect to the thermocline while the temperature vs depth profile is static. There can be important consequences for acoustic ray tracing at ray turning points that depend on the direction of propagation.

DIRECTIONAL WAVE SPECTRUM OF SEA SURFACE ACOUSTICAL METHOD

Fig. VII-3

(A) ONE-DIMENSIONAL WAVE HEIGHT POWER SPECTRUM

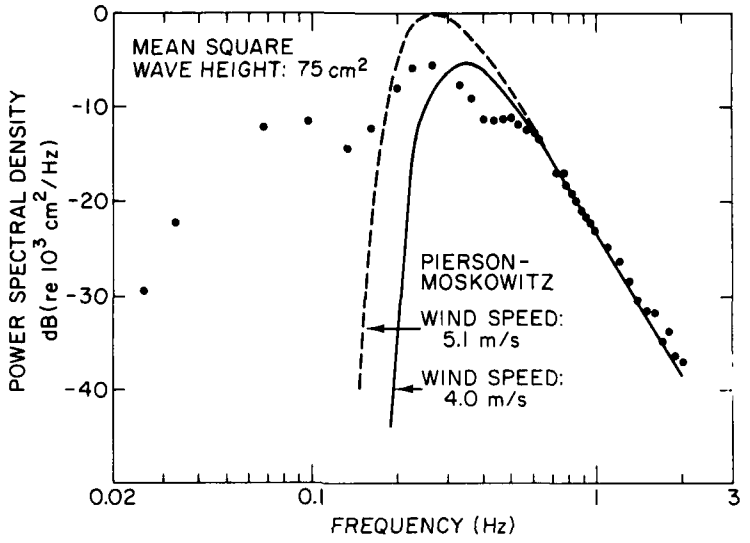

(B) DIRECTIONALITY SPECTRA

(ARRAY LENGTH: 274.3 cm)

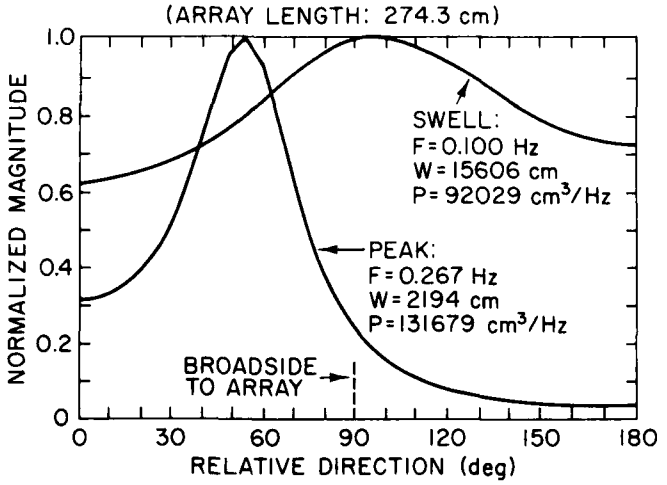

(ADAPTED FROM RODERICK: 1979)

VERTICAL PROFILE OF THE HORIZONTAL CURRENT FIELD

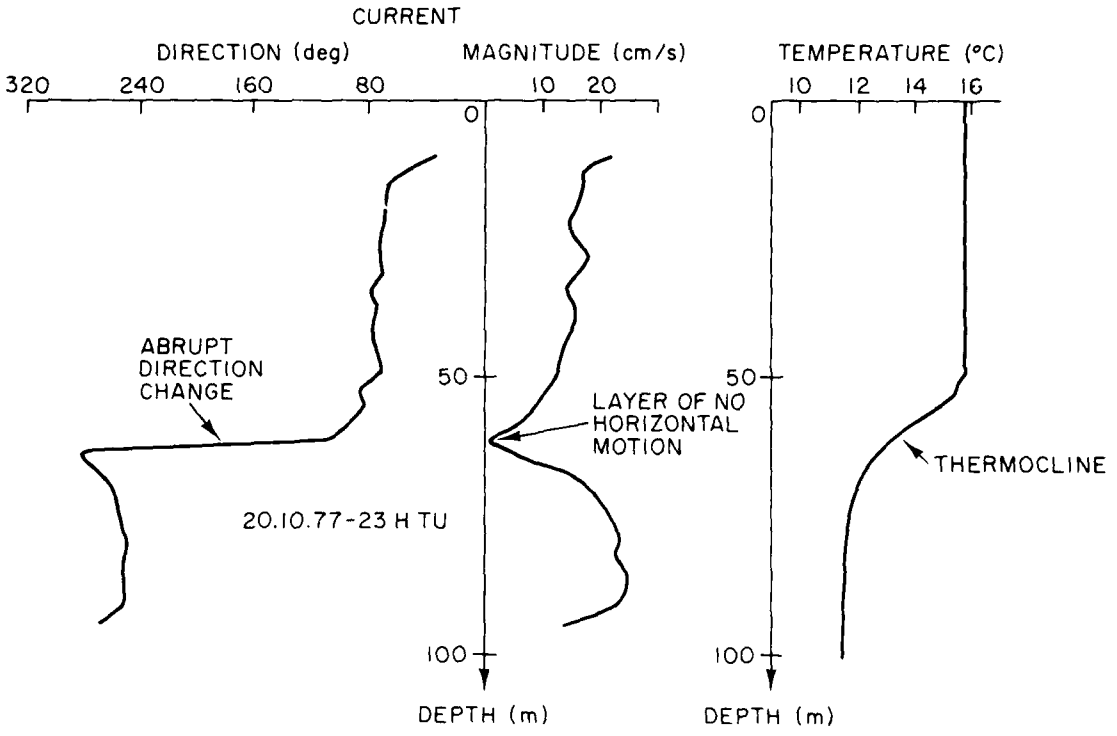

Fig. VII-4

(Peynaud and Pijanowski: 1979)

VIII. OCEAN DYNAMICS -- FINESTRUCTURE AND MICROSTRUCTURE

Figure VIII-1: Example of Finestructure Detail

Layers of the order of tens of meters in the vertical down to about a half-meter occur in the finestructure region of the turbulence decay spectrum. In this figure (Ref. VIII-1), a section of the temperature vs depth plot has been processed to show finestructure activity. A thermocline is shown with much thermal activity as is indicated by the wiggles in the temperature gradient plot. The activity of finestructure is really brought out if the vertical temperature gradient is squared and half-meter averages plotted. The ratio of the mean square temperature gradient to the mean temperature gradient squared is called the Cox Number. The Cox Number measures the heat flow and is equal to the ratio of the eddy thermal conductivity to the molecular thermal conductivity.

Figure VIII-2: Finestructure and Microstructure Acoustics

This figure was obtained by Hess and Orr recording as a function of time the scattered return of energy at 200 kHz. The WHOI multifrequency sonar system (20, 100, 200, 300, 500 kHz) (Ref. VIII-2) was towed from a slowly moving ship. Note the extremely complicated temperature vs depth profile superposed in white in the center of the figure. The scattering returns outline the layering and result from the extremely fine particulates, both organic and inorganic, which are caught up in the ocean's dynamical processes. A total particulate content of 60 μg/ℓ was sampled at 90 m.

Figure VIII-3: Frequency Dependence of Four Backscattering Mechanisms

Orr and Hess have embarked on a program to study the fluidic processes in the internal wave, finestructure and microstructure regions by studying the frequency dependence of the scattering mechanisms (Ref. VIII-3). The figure shows the expected acoustic pressure dependence for four of these mechanisms. One of their tasks will require the determination of the size distribution of the scatterers which will "color" the frequency dependence.

Figure VIII-4: Separation of Layered and Point Scatterers

Kaye and Anderson (Ref. VIII-4) have used wavefront analysis for measurements from a large aperture array at 8 kHz to distinguish between layered and point scatterers. Note in the figure that at some depths one type or the other predominates, while at other depths both types of scattering are present.

EXAMPLE OF FINESTRUCTURE DETAIL:

A THERMOCLINE PORTION OF FINESTRUCTURE

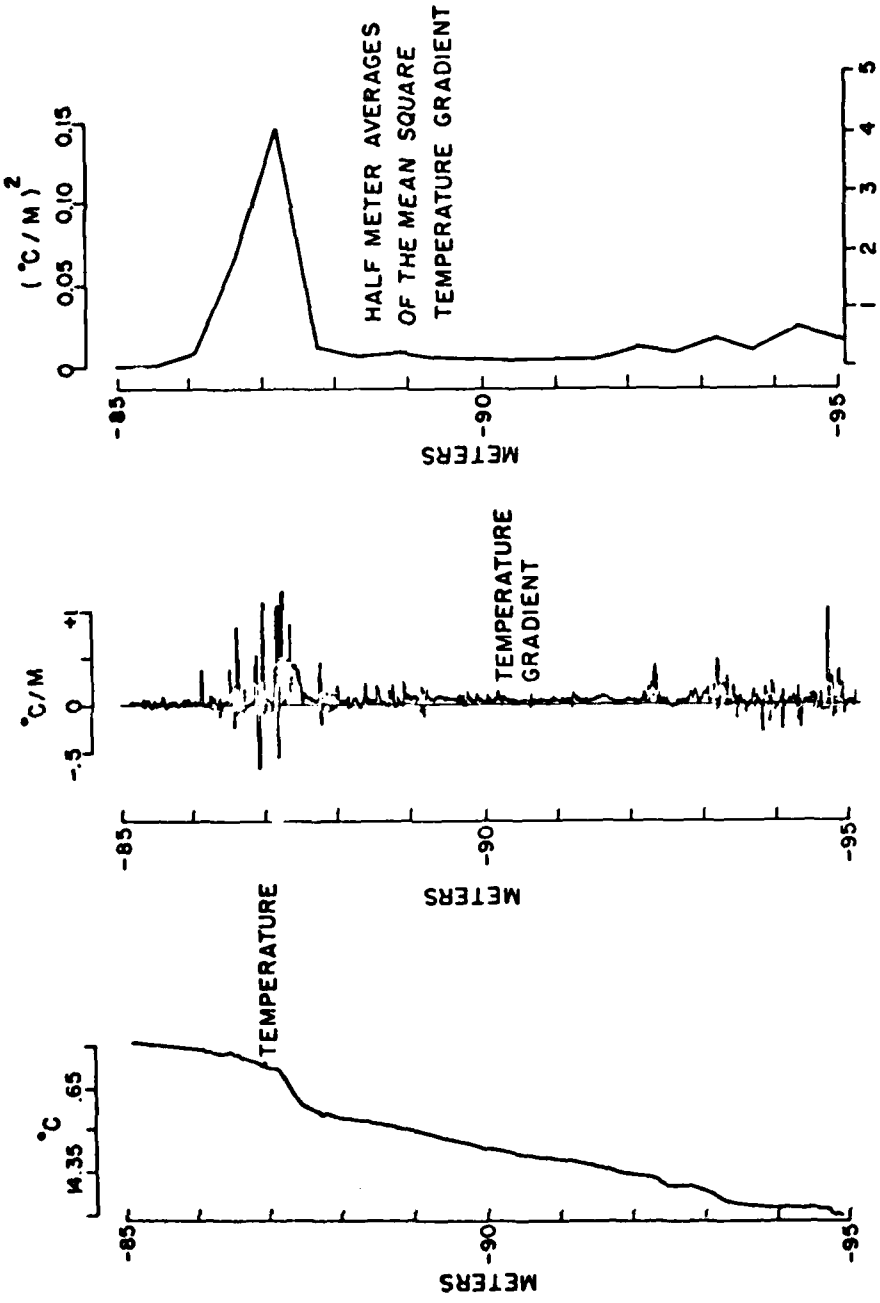

(Gregg: 1973)

Fig.
VIII-1

Fig.
VIII-2

FINESTRUCTURE ACOUSTICS -- WATER MASSES AT WORK IN HUDSON CANYON

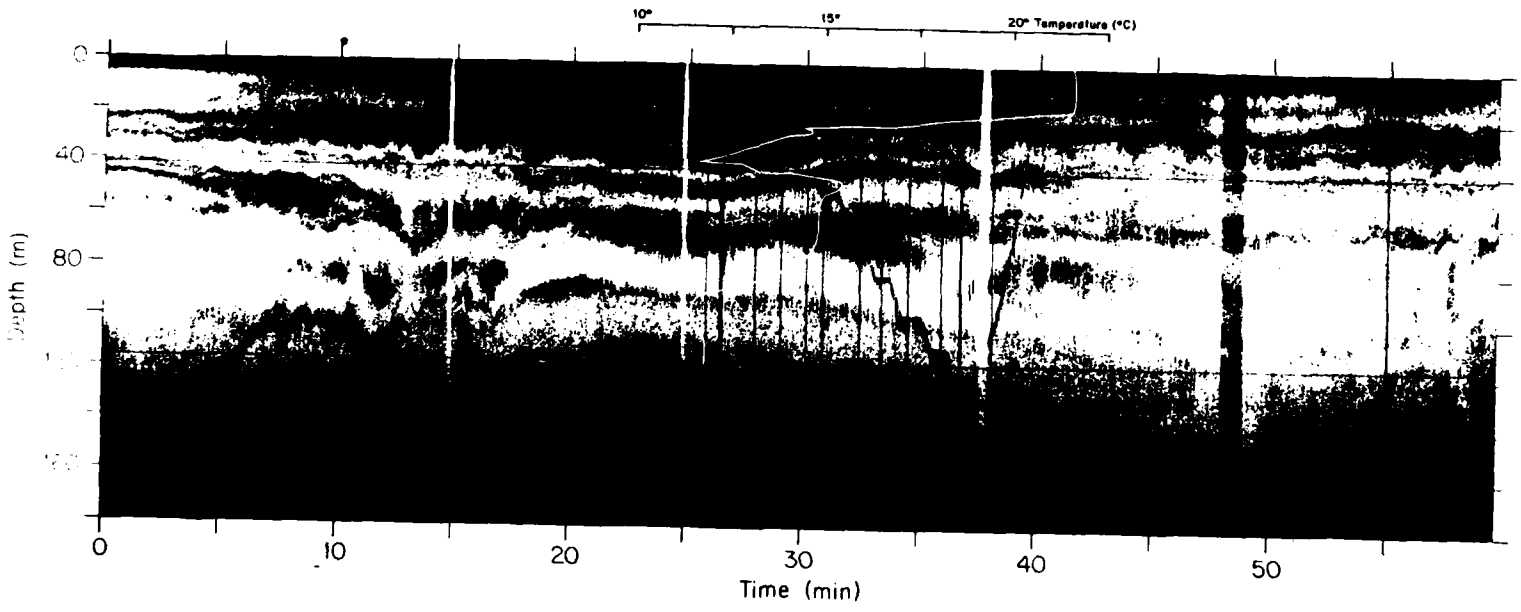

(Hess and Orr: 1979)

FREQUENCY DEPENDENCE OF FOUR BACKSCATTERING MECHANISMS

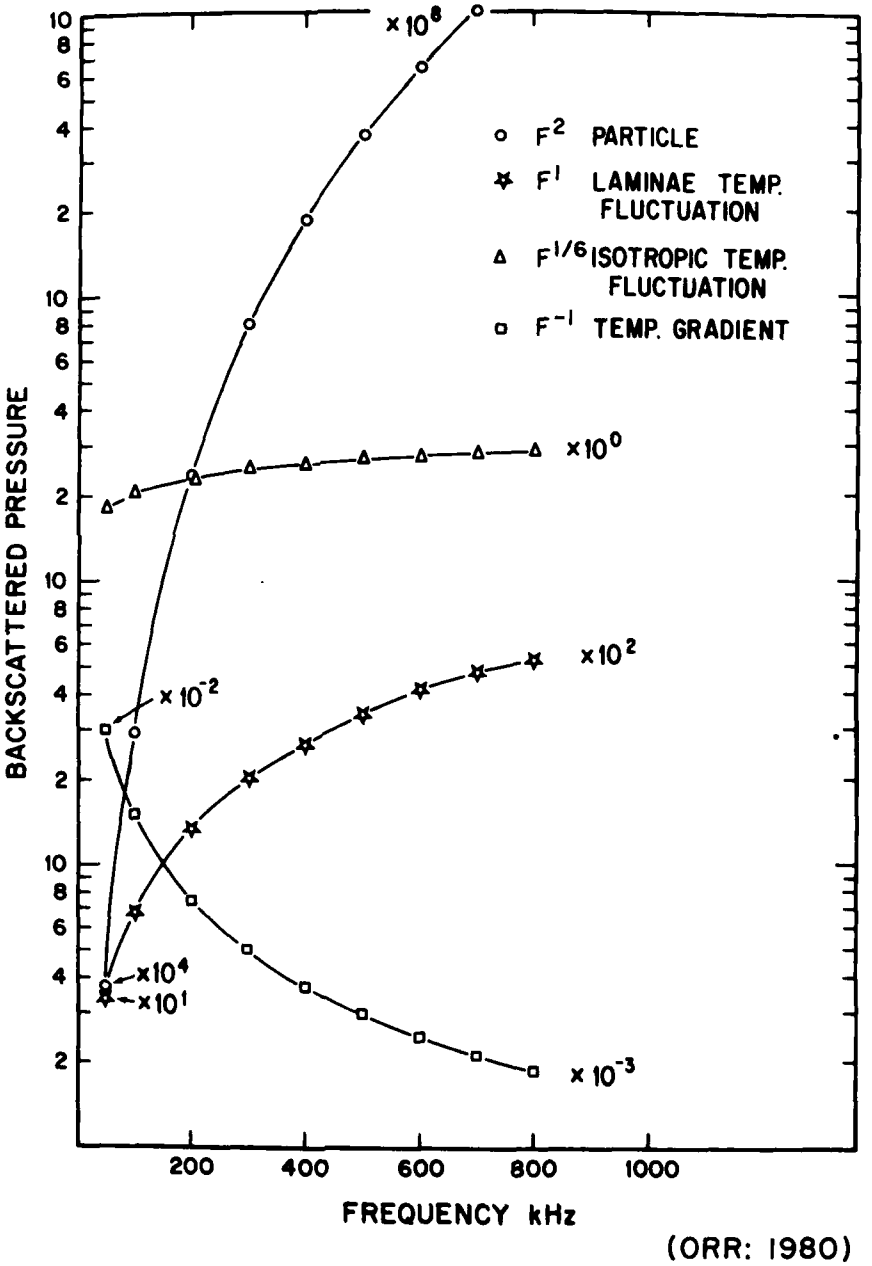

(ORR: 1980)

Fig. VIII-3

SEPARATION OF LAYERED AND POINT SCATTERERS

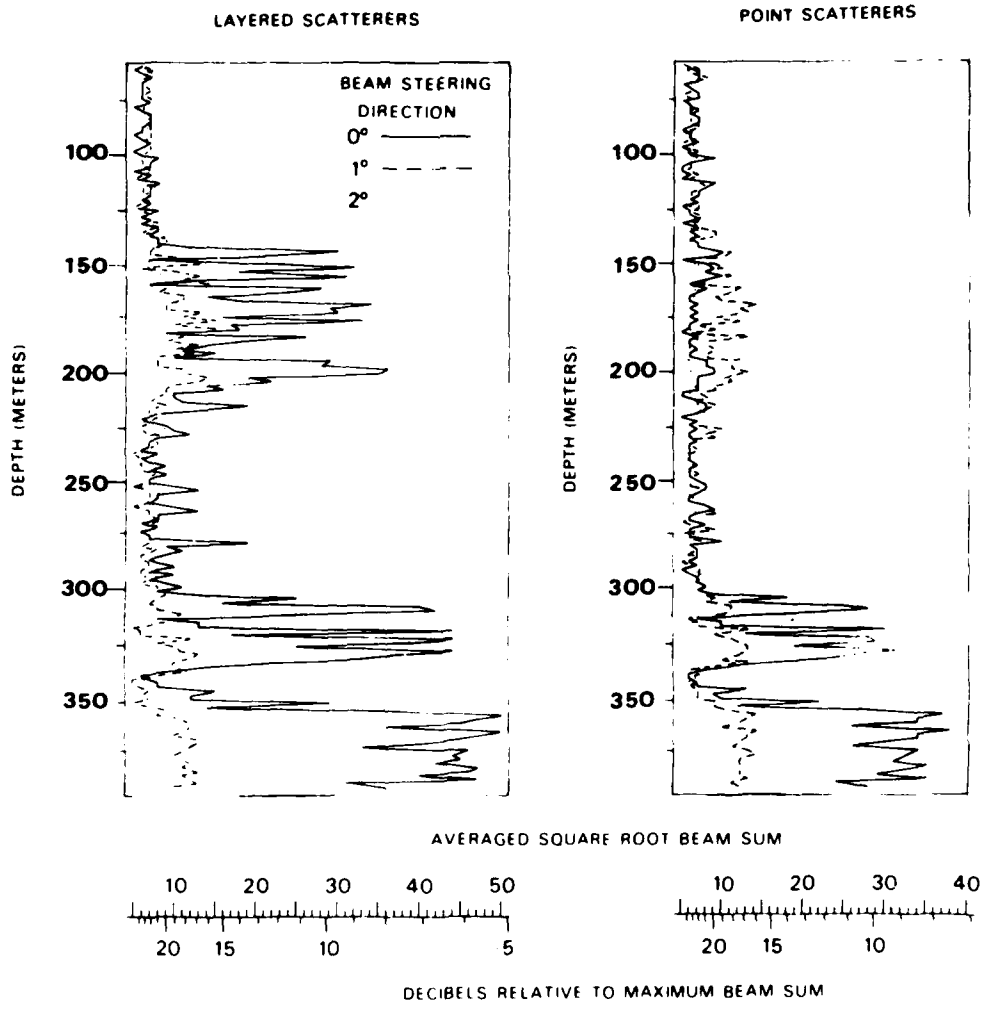

Fig. VIII-4

(Kaye and V. Anderson: 1979)

IX. CONCLUSIONS *In the next ten years:*

1. Ocean acoustic remote sensing techniques and systems will be developed for studying ocean dynamics on all scales. These investigations will be spurred by the efficiency of experimental design enabled by satellite oceanography as a reconnaissance tool.

2. Synoptic scale and mesoscale features will be monitored by using long fixed paths and measuring time variability in travel time, intensity and doppler shifts for identifiably-coded ray paths as they traverse different sections of the ocean both in the vertical and horizontal. Acoustic tomography is one of the key tools here.

3. Finestructure and microstructure configurations and mixing processes will be studied intensively since they are bite size and can be carried out using presently developed high frequency acoustic systems. The study of how particulates, both organic and inorganic, mimic such features will be emphasized. Acoustic frequency dependence will play an important role.

4. The measurement and study of currents and shear profiles will be emphasized in the study of ocean dynamics and heat transfer and their relations to climate and weather, navigation, transportation, and the dispersion of pollutants and fisheries nutrients.

5. Acoustic transmissometers will be developed for joint use with optical transmissometers for in situ studies of states of particulate aggregations and suspension for sedimentation information as well as upwelling of nutrients. The satellite coastal zone color scanner will be useful for reconnaissance.

6. Acoustic remote sensing techniques will be used to study wind stress, temperature profiles and directional wave spectra from bottom-mounted and buoyed systems.

7. There will be much greater development and use of sophisticated sonar for counting, integration, and mapping techniques for the problems of fishery stock assessment as well as for fishing itself.

8. The details of the bottom will be explored more fully by intricate sonar for exploitation of mineral resources. Acoustic devices will be developed for monitoring sea floor spreading and for subbottom holography.

REFERENCES

(mostly for figure credits)

I. Introduction

1. "NOAA Workshop on Oceanic Remote Sensing," Estes Park Colorado, August 19-24, 1979, John W. Sherman III (Ed.).

   (a) Volume I - Action Summary and Report, December 1979.
   (b) Volume II - Workshop Support Documentation, March 1980.

2. "NOAA Workshop on Ocean Acoustic Remote Sensing," Seattle, Washington, January 21-24, 1980. S.R. Murphy and M. Schulkin (Eds.).

   (a) Volume I - Summary Report, March 1980.
   (b) Volume II - Presentations and Working Group Reports, April 1980.

3. "NASA Oceanic Processes Program--Status Report - Fiscal Year 1980," W.S. Wilson, NASA Tech. Memo 80233, July 1980.

4. "Conferences on the National Oceanic Satellite System (NOSS)," May 19 - June 5, 1980, NOAA-NESS. Part I: NOAA's Mission and Satellite Experience. Part II: NOSS Description.

II. Marine Geology and Ocean Depths

1. "Hydrographic Reconnaissance of Large Undersea Topography Using Scattered Acoustic Energy," D. Schifter, E. Franchi, J. Griffin and B. Adams, J. Acoust. Soc. Am. 66, S25, 1979.

2. "Kane 9. Global Ocean Floor Analysis and Research Data Series," A. Lowrie and E. Escowitz, U.S. Naval Oceanographic Office, 1969.

3. See Ref. I-2-b, Paper #11, "Ocean Acoustic Remote Sensing of the Sea Floor," F.N. Spiess.

4. "Acoustical Oceanography," C.S. Clay and H. Medwin, John Wiley and Sons, NY, 1977, p. 354.

III. Ocean Chemistry and Pollution

1. "Remote Sensing Techniques for the Location and Measurement of Shallow-Water Features," F.A. Polcyn and R.A. Rollin, Infrared and Optical Sensor Laboratory, Willow Run Laboratories, The Institute of Science and Technology, University of Michigan, January 1969.

2. See Ref. I-2-b, Paper #10, "Ocean Acoustics and Chemistry," F.H. Fisher.

3. "The Potential Application of Remote Sensing in Chemical Oceanographic Research," N.R. Anderson, ONR West #80-1, ONR Scientific Liaison Office, Scripps Institution of Oceanography, June 1980.

4. "Optical Aspects of Oceanography," N.G. Jerlov and E.S. Nielsen (Eds.), Academic Press, NY, 1974. See Chapter 2: Observed and Computed Scattering Functions, by G. Kullenberg.

5. "Acoustic Tracking of Ocean-Dumped Sewage Sludge," J.R. Proni, F.C. Newman, R.L. Sellers, and C.A. Parker, Science 193, 1005-1007, 1976.

6. "Oceanography and Underwater Sound for Naval Applications," SP-84, U.S. Naval Oceanographic Office, Washington, D.C., 1966.

See also

7. "Suspended Solids in Water," R.J. Gibbs (Ed.), Plenum Press, NY, 1974.

8. See Ref. I-2-b, Papers #8, #9, and #12:
"Marine Pollution and Ocean Acoustic Remote Sensing: Requirements," C.A. Parker and R.L. Swanson.
"On the Use of Acoustics in Oceanic Pollution Problems," J.R. Proni.
"Remote Acoustic Sensing of Oceanic Fluid and Biological Processes," M.H. Orr.

IV. Biomass and Fisheries

1. "Maximum Side-Aspect Target Stength of an Individual Fish," R.H. Love, J. Acoust. Soc. Am. 46, 746-752, 1969.

2. "Proceedings of an International Symposium on Biological Sound Scattering in the Ocean," G. Brooke Farquhar (Ed.), GPO #0851-0553, Government Printing Office, Washington, D.C., 1970.

"A Reconnaissance of the Deep Scattering Layers in the Eastern Tropical Pacific and the Gulf of California," C.R. Dunlap, pp. 395-408.

3. "Acoustic and Environmental Knowledge for Biological False Target Prediction," R.H. Love, R.S. Winokur and C. Levenson, NAVOCEANO TN #6130-8-74, July 1974.

4. "Meeting on Hydroacoustical Methods for the Estimation of Marine Fish Populations," 25-29 June 1979, Charles Stark Draper Laboratory, Inc., Cambridge, MA.

Volume I - Findings of the Scientific and Technical Specialists: A Critical Review.

5. "Fish School Acoustic Target Strength," I.E. Davies, R.J. Vent and J.C. Brown, J. Cons. Int. Explor. Mer 37, 288-292, 1977.

6. "Doppler Structure in Echoes from Schools of Pelagic Fish," D.V. Holliday, J. Acoust. Soc. Am. 55, 1313-1322, 1974.

See Also

7. Ref. I-2-b, Paper #7, "Acoustical Techniques in Fisheries Resource Management," P.H. Moose.

V. Ocean Dynamics -- Macroscale, Synoptic Scale, and Mesoscale

1. "Variability of the Oceans," A.S. Monin, V.M. Kamenkovich and V.G. Kort, John Wiley and Sons, 1977.

2. "Long-Period Fluctuations of CW Signals in Deep and Shallow Water," J.G. Clark and M. Kronengold, J. Acoust. Soc. Am. 56, 1071-1083, 1974.

3. "Ocean Acoustic Tomography: A Scheme for Large Scale Monitoring," W. Munk and C. Wunsch, Deep-Sea Research 26A, 123-161, 1979.

4. See Ref. I-2-b, Paper #4, "Ocean Acoustic Tomography: A Method for Measuring Large-Scale Variability," W.H. Munk.

VI. Ocean Dynamics -- Internal Waves and Tides

1. "Sound Transmission Through a Fluctuating Ocean," S.M. Flatté (Ed.), Cambridge University Press, 1979.

2. "Statistical Description of Internal Waves and Temperature Fine Structure in the Deep Ocean," M.R. Levine, Ph.D. Thesis, University of Washington, Seattle, WA, 1979.

3. "A Numerical Simulation of the Effects of Oceanic Finestructure on Acoustic Transmission," T.E. Ewart, J. Acoust. Soc. Am. 67, 496-503, 1980.

VII. Ocean Dynamics -- The Sea Surface and Near-Surface Layer

1. "On Monitoring Depth Variations of the Main Thermocline Acoustically," T. Rossby, J. Geophys. Res. 74, 5542-5546, 1969.

2. "Measuring Dynamic Heights with Inverted Echo Sounders: Results from MODE," D.R. Watts and H.T. Rossby, J. Phys. Oceanogr. 7, 345-358, 1977.

3. "The Inverted Echo Sounder," D.S. Bitterman Jr. and D.R. Watts, OCEANS '79, Conference Proceedings, IEEE Ref. Pub. 79CH1478-7 OEC, pp. 302-306, Sept. 1979.

4. See Ref. I-2-b Paper #13, "Estimation of Wind Speed and Stress at the Sea Surface from Ambient Noise Measurements," D.R. Watts.

5. "On the Estimation of Oceanic Wind Speed and Stress from Ambient Noise Measurements," P.T. Shaw, D.R. Watts and H.T. Rossby, Deep-Sea Research 25, 1225-1233, 1978.

6. "Doppler Spectra of Bistatic Reverberation from the Sea Surface," W.I. Roderick, NUSC TR6031, Naval Underwater Systems Center, New London, CT, May 1979.

7. "An Acoustic Doppler Current Meter," F. Peynaud and J. Pijanowski, Offshore Technology Conference, April 30 - May 3, 1979, Houston, TX, pp. 863-874.

8. "Observations of Strongly Nonlinear Internal Motion in the Open Sea Using a Range-Gated Doppler Sonar," R. Pinkel, J. Phys. Oceanogr. 9, 675-686, 1979.

9. "Velocity Measurement using Correlation Sonar," F.R. Dickey and J.A. Edward, IEEE PLANS-78, Position, Location and Navigation Symposium, pp. 255-264.

VIII. Ocean Dynamics -- Finestructure and Microstructure

1. "The Microstructure of the Ocean," M.C. Gregg, Sci. Am. 228, 65-77, 1973.

2. "A Towed, Multifrequency H.F. Sonar System for Scattering and Ocean Dynamics Studies," F.R. Hess and M.H. Orr, WHOI Tech. Rpt. 79-76, Woods Hole Oceanographic Institution, Woods Hole, MA, October 1979.

3. "Remote Acoustic Sensing of Oceanic Fluid and Biological Processes," M.H. Orr, WHOI-80-2, Woods Hole Oceanographic Institution, Woods Hole, MA, June 1980.

4. "Scattering from Oceanic Microstructure: Detection with a Large Aperture Array," G.T. Kaye and V.C. Anderson, J. Acoust. Soc. Am. 66, 842-849, 1979.